Author/s:
Mellergaard, M;Høgh, RI;Lund, A;Aldana, BI;Guérillot, R;Møller, SH;Hayes, AS;Panagiotopoulou, N;Frimand, Z;Jepsen, SD;Hansen, CHF;Andresen, L;Larsen, AR;Peleg, AY;Stinear, TP;Howden, BP;Waagepetersen, HS;Frees, D;Skov, S

Title:
Staphylococcus aureus induces cell-surface expression of immune stimulatory NKG2D ligands on human monocytes

Date:
2020-08-14

Citation:
Mellergaard, M., Høgh, R. I., Lund, A., Aldana, B. I., Guérillot, R., Møller, S. H., Hayes, A. S., Panagiotopoulou, N., Frimand, Z., Jepsen, S. D., Hansen, C. H. F., Andresen, L., Larsen, A. R., Peleg, A. Y., Stinear, T. P., Howden, B. P., Waagepetersen, H. S., Frees, D. & Skov, S. (2020). Staphylococcus aureus induces cell-surface expression of immune stimulatory NKG2D ligands on human monocytes. Journal of Biological Chemistry, 295 (33), pp.11803-11821. https://doi.org/10.1074/jbc.ra120.012673.

Persistent Link:
https://hdl.handle.net/11343/273804

Staphylococcus aureus induces cell-surface expression of immune stimulatory NKG2D ligands on human monocytes

Received for publication, January 21, 2020, and in revised form, June 24, 2020 Published, Papers in Press, June 30, 2020, DOI 10.1074/jbc.RA120.012673

Maiken Mellergaard[1], Rikke Illum Høgh[1], Astrid Lund[1], Blanca Irene Aldana[2], Romain Guérillot[3], Sofie Hedlund Møller[1], Ashleigh S. Hayes[3], Nafsika Panagiotopoulou[1], Zofija Frimand[1], Stine Dam Jepsen[1], Camilla Hartmann Friis Hansen[1], Lars Andresen[1], Anders Rhod Larsen[4], Anton Y. Peleg[5,6], Timothy P. Stinear[3], Benjamin P. Howden[3], Helle S. Waagepetersen[2], Dorte Frees[7], and Søren Skov[1,*]

From [1]Experimental Animal Models and [7]Food Safety and Zoonosis, Department of Veterinary and Animal Sciences, Faculty of Health and Medical Sciences and the [2]Department of Drug Design and Pharmacology, Faculty of Health and Medical Sciences, University of Copenhagen, Copenhagen, Denmark, the [3]Department of Microbiology and Immunology, University of Melbourne at the Doherty Institute for Infection and Immunity, Melbourne, Victoria, Australia, the [4]Statens Serum Institut, Microbiology and Infection Control, Copenhagen, Denmark, and the [5]Department of Infectious Diseases, Alfred Hospital and Central Clinical School and the [6]Infection and Immunity Program, Monash Biomedicine Discovery Institute and Department of Microbiology, Monash University, Melbourne, Victoria, Australia

Edited by Chris Whitfield

***Staphylococcus aureus* is among the leading causes of bacterial infections worldwide. The pathogenicity and establishment of *S. aureus* infections are tightly linked to its ability to modulate host immunity. Persistent infections are often associated with mutant staphylococcal strains that have decreased susceptibility to antibiotics; however, little is known about how these mutations influence bacterial interaction with the host immune system. Here, we discovered that clinical *S. aureus* isolates activate human monocytes, leading to cell-surface expression of immune stimulatory natural killer group 2D (NKG2D) ligands on the monocytes. We found that expression of the NKG2D ligand ULBP2 (UL16-binding protein 2) is associated with bacterial degradability and phagolysosomal activity. Moreover, *S. aureus*–induced ULBP2 expression was linked to altered host cell metabolism, including increased cytoplasmic (iso)citrate levels, reduced glycolytic flux, and functional mitochondrial activity. Interestingly, we found that the ability of *S. aureus* to induce ULBP2 and proinflammatory cytokines in human monocytes depends on a functional ClpP protease in *S. aureus*. These findings indicate that *S. aureus* activates ULBP2 in human monocytes through immunometabolic mechanisms and reveal that *clpP* inactivation may function as a potential immune evasion mechanism. Our results provide critical insight into the interplay between the host immune system and *S. aureus* that has evolved under the dual selective pressure of host immune responses and antibiotic treatment. Our discovery of an immune stimulatory pathway consisting of human monocyte-based defense against *S. aureus* suggests that targeting the NKG2D pathway holds potential for managing persistent staphylococcal infections.**

The commensal bacterium *Staphylococcus aureus* is a major cause of infections ranging from superficial skin infections to life-threatening diseases like sepsis, endocarditis, and osteomyelitis (1). Treatment of *S. aureus* mainly relies on antibiotics, a strategy that is challenged by the ability of *S. aureus* to develop antibiotic resistance (2). The most crucial antimicrobial resistance issue in *S. aureus* has been the evolution and dissemination of methicillin-resistant *S. aureus* (MRSA) strains (3). MRSA infections are typically treated with last-line antibiotics, such as daptomycin or vancomycin (4, 5). The emergence of daptomycin-resistant *S. aureus* isolates is associated with spontaneous genetic changes that also seem to impact bacterial virulence and enhance the risk of chronic infections (4, 6). Thus, the dual selective pressure of daptomycin and the immune system may select for mutations that render the bacterium less susceptible to the antibiotic while increasing immune evasion and persistent infections. The NKG2D receptor-ligand system is a key immune sensing mechanism involved in detection of infection, inflammation, and malignant cells (7, 8). The activating NKG2D receptor is expressed in a number of immune effector cells, in particular $CD8^+$ T cells and natural killer cells (9). NKG2D interacts with eight different NKG2D ligands that can be induced on the cell surface of stressed cells (10, 11). NKG2D ligands are divided into two families: the major histocompatibility complex class I–related family containing polymorphic MICA and MICB and the UL16-binding protein family consisting of ULBP1–6 (9, 10). NKG2D ligand-receptor engagement leads to cytokine release, degranulation, immune cell activation, and influence specificity of the immune response (7, 12). Cancer and virus-infected cells can evade immune recognition by obstructing cell-surface expression of NKG2D ligands (13, 14). We previously showed that *N*-glycosylation is important for cell-surface expression of MICA and that U21 expressed by herpesvirus-7 blocked allele-specific MICA surface expression through altered *N*-glycosylation (15, 16). Monocytes are involved in the early defense against a number of microbial infections (17, 18). The response to *S. aureus* is mediated through phagocytosis, intracellular degradation, and cytokine secretion (19–22). Human monocytes express Toll-like receptor 2 (TLR2) that is involved in the staphylococcal response, and stimulation by *S. aureus* or purified peptidoglycan (PGN) induces expression

This article contains supporting information.

* For correspondence: Søren Skov, sosk@sund.ku.dk.

of tumor necrosis factor α, IL-1β, IL-6, and IL-10 (23–26). Phagocytosis and intracellular degradation release bacterial components, which are sensed by a number of cytoplasmic receptors (27). Because of antibiotic exposure, many staphylococcal strains carry cell wall modifications like increased PGN cross-linking and *O*-acetylation that have profound effects on degradability, inflammation, and immunity (28, 29).

In this study, we investigated immunity to a series of isogenic MRSA strains isolated from the blood of a patient with persistent bloodstream infection undergoing daptomycin treatment. Daptomycin targets the bacterial cell envelope, and during treatment the infecting MRSA isolate acquired a number of single-nucleotide polymorphism (SNPs) that rendered the new strains less susceptible to daptomycin (6, 30). We find that human monocytes in response to *S. aureus* induce expression of NKG2D ligands through increased transcription. Mechanistically, we show that the up-regulation of the NKG2D ligand ULBP2 associates with lysozyme susceptibility of *S. aureus* and phagolysosomal activity in monocytes. Daptomycin exposure led to mutations in the *rpoB* and *clpP* genes, resulting in a thickened bacterial cell wall and increased resistance to lysosomal degradation, and we show that a mutation in the highly conserved *S. aureus clpP* gene hampered ULBP2-mediated immune activation and secretion of proinflammatory cytokines. Finally, we show that *S. aureus* mediates a metabolic change of monocytes characterized by lowered glycolysis and elevated intracellular level of (iso) citrate that is likely causally involved in NKG2D ligand regulation, because citrate and inhibitors of glycolysis directly induce ULBP2 expression in monocytes. Our study describes induction of NKG2D ligands by *S. aureus* on human monocytes and furthermore connects *S. aureus* with an altered metabolic phenotype causing surface expression of ULBP2 in human monocytes.

Results

S. aureus induces cell-surface expression of NKG2D ligands on human monocytes

We investigated NKG2D ligand expression in response to five clinical MRSA strains, SADR-1–SADR-5 (6). The strains developed reduced susceptibility to daptomycin via acquisition of SNPs in *rpoB*, *clpP*, *clpX*, *mprF*, and other genes (Fig. 1*A*). We previously described the contribution of the individual SNPs to antibiotic resistance and fitness of strains SADR-1–SADR-4 (30). SADR-5 was isolated from the same patient and shares the SNP in *rpoB*; however, it has four additional SNPs not present in SADR-2–SADR-4 (Fig. 1*A*).

We stimulated human monocytes (THP1 cells) with UV-killed *S. aureus* SADR-1–SADR-5 and assessed NKG2D ligand surface expression by flow cytometry after 12, 24, and 48 h. Upon *S. aureus* exposure, we found that ULBP2 was induced on the surface of THP1 with expression increasing over time (Fig. 1*B*). Interestingly, SADR-1 and SADR-5 induced a pronounced ULBP2 response compared with SADR-2–SADR-4 (Fig. 1, *B* and *C*). In addition, we examined ULBP2 expression after exposure to another MRSA strain USA300JE2 and found this was as potent as SADR-1 and SADR-5 in inducing ULBP2 in THP1 cells (Fig. 1, *B* and *C*). Furthermore, USA300JE2 and SADR-1 induced ULBP2 in a dose-dependent manner (Fig. S1*A*). Of note, expression of the NKG2D ligands MICA/B, ULBP1, ULBP3, and ULBP4 was not affected by exposure to any of the *S. aureus* strains in THP1 cells (Fig. S1, *B* and *C*). ULBP2 mRNA levels were significantly induced in monocytes exposed to SADR-1, SADR-5, and USA300JE2 for 24 h, whereas induction was lower in monocytes exposed to SADR-2–SADR-4 (Fig. 1*D*), corresponding to the observed ULBP2 surface expression (Fig. 1, *B* and *C*). To further verify the NKG2D ligand response to S. *aureus*, we investigated NKG2D ligand expression in primary monocytes. As shown in Fig. 1*E*, ULBP2 transcription was increased in SADR-1–treated primary monocytes after 4 and 8 h. Interestingly, we saw that also MICA/B transcription and surface expression were increased in these cells (Fig. S1, *D* and *E*), whereas no surface expression was detected for ULBP1, ULBP3, and ULBP4 (Fig. S1*F*). The absence of MICA/B expression in THP1 cells is likely explained by a specific defect in these cells, in line with previous findings (31). Moreover, we saw a high donor variation in expression of the individual NKG2D ligands, an observation previously described in human monocytes (32).

We tested ULBP2 expression in response to live SADR-1 and USA300JE2. Consistent with our data using UV-killed strains, live *S. aureus* significantly increased expression of ULBP2 on both the surface (Fig. 1*F*) and mRNA levels (Fig. 1*G*). The response was even more potent for live USA300JE2 compared with UV-killed (Fig. 1*G*), likely because of bacteria proliferating within the monocyte culture medium in accordance with the observed dose-dependent ULBP2 induction by UV-killed strains (Fig. S1*A*). Together, these data show that *S. aureus* induces transcriptional expression of NKG2D ligands, ULBP2 in THP1 and primary monocytes, and ULBP2 and MICA/B in primary monocytes.

We next investigated the functional outcome of the *S. aureus*–mediated ULBP2 expression. First, we used a soluble NKG2D-Fc receptor to assess whether *S. aureus*–induced ULBP2 expression promoted binding to the NKG2D receptor. As shown in Fig. 2*A*, the soluble NKG2D receptor interacted with monocytes in a pattern that correlated with ULBP2 expression (Figs. 1*C* and 2*B*).

The data demonstrate that *S. aureus* induces ULBP2 expression on THP1 cells and that the mutations in *rpoB* and *clpP* acquired in SADR-2 during exposure to daptomycin reduce the ability to induce ULBP2. Mutations in *rpoB* are associated with the global emergence of stable, multidrug-resistant staphylococcal lineages (33, 34), whereas the highly conserved *clpP* is important for stress tolerance and virulence. Interestingly, ClpP exerts many of its functions through interaction with ClpX (35). We find it intriguing that these mutations also impact the ability of *S. aureus* to cause immune activation by modifying surface expression of ULBP2 on monocytes and therefore focused primarily on SADR-1 and SADR-2 in the remainder of this study.

SADR-2 fails to induce NKG2D-mediated immune response compared with SADR-1

Next, we examined whether induced ULBP2 resulted in signaling through the NKG2D receptor. We used an established 2B4 cell line that expresses GFP in response to NFAT (nuclear

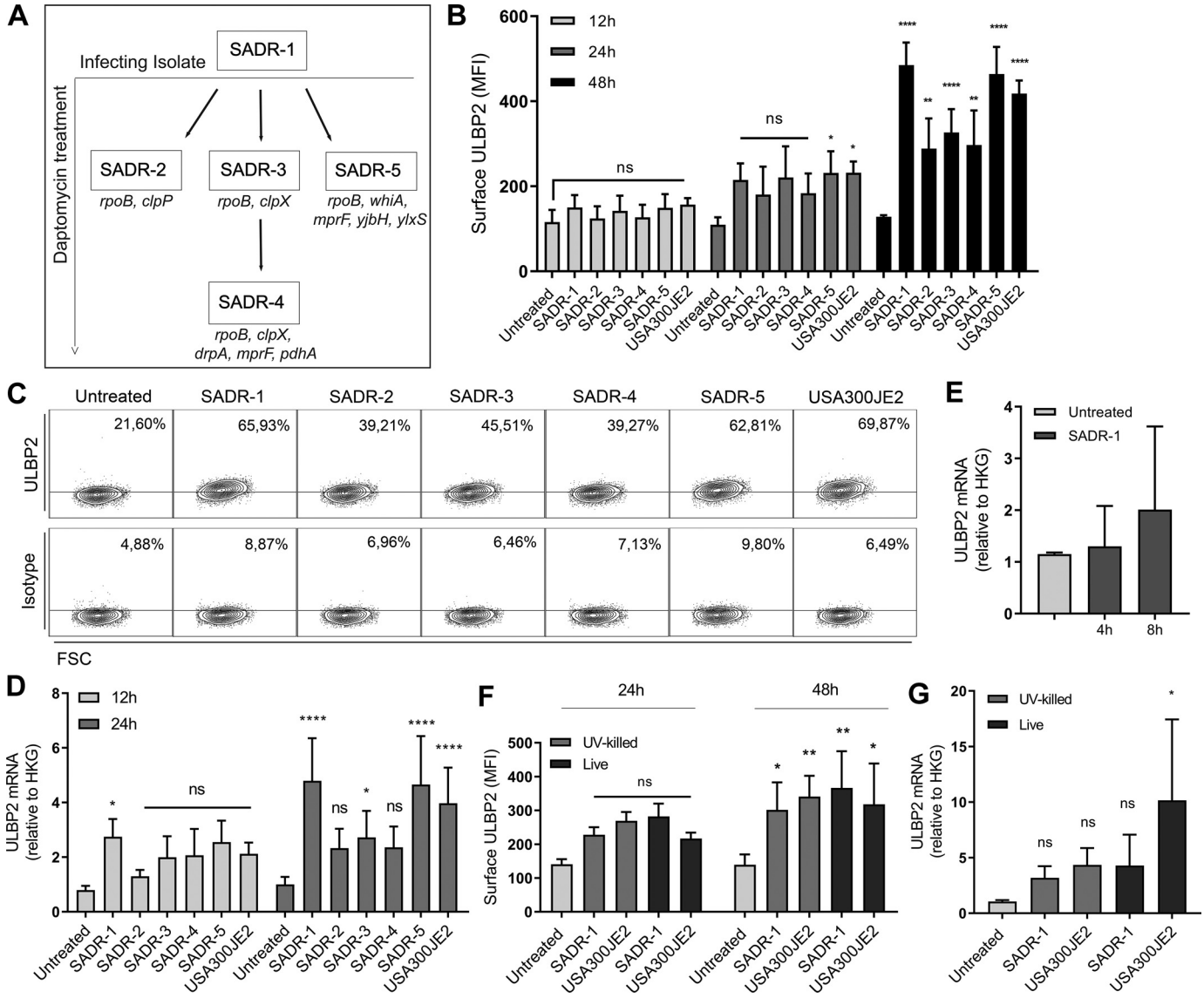

Figure 1. *S. aureus* induces cell-surface expression of ULBP2 on human monocytes. *A*, schematic overview of the clinical, isogenic *S. aureus* strains SADR-1–SADR-5 used in this study. *Arrows* represent acquired SNPs and decreasing daptomycin susceptibility that the isolates have gained at each step in their developmental path. SADR-1 is the infecting isolate. SADR-2 and SADR-3 have decreased susceptibility to daptomycin, whereas SADR-4 and SADR-5 are daptomycin-resistant. Resequencing isolates revealed a mutation in *clpP* G94D in SADR-2 not previously reported (6, 30). *B*, human THP1 cells were treated with SADR-1–SADR-5, USA300JE2, or PBS (untreated). Surface expression of ULBP2 was analyzed after 12, 24, and 48 h by flow cytometry. *C*, THP1 cells were treated with SADR-1–SADR-5 or USA300JE2. Surface expression of ULBP2 and isotype background were analyzed after 48 h by flow cytometry. Dot plots show percentage ULBP2 surface expression (*upper row*) and isotype staining (*lower row*) and are representative of three independent experiments. *D*, THP1 cells were treated with SADR-1–SADR-5 or USA300JE2. Total RNA was purified after 12 and 24 h and analyzed for ULBP2 expression by quantitative real-time PCR. *E*, human primary monocytes were treated with SADR-1. Total RNA was purified after 4 and 8 h and analyzed for ULBP2 expression by quantitative real-time PCR. *F*, THP1 cells were treated with UV-killed or live SADR-1 or USA300JE2. Surface expression of ULBP2 was analyzed after 24 and 48 h by flow cytometry. *G*, THP1 cells were treated with UV-killed or live SADR-1 or USA300JE2. Total RNA was purified after 24 h and analyzed for ULBP2 expression by quantitative real-time PCR. The data are presented as follows: *B* and *F* show surface expression as MFI ± S.D. of data from three independent experiments; *D* and *G* show data from four or three independent experiments, respectively, presented as fold change ± S.D. of ULBP2 mRNA normalized to HKG; *E* shows data from three independent experiments (two for untreated sample) presented as ULBP2 mRNA normalized to HKG ± S.D. Statistical analysis was performed by two-way ANOVA with Tukey's multiple comparisons test for data in *B*, *D*, and, *F* and one-way ANOVA with Dunnett's multiple comparisons test for data in *G*. Statistics are presented relative to untreated control. *FSC*, forward scatter; *ns*, not significant.

factor of activated T cell) activity, and the reporter cells were further transfected with or without human NKG2D/DAP10-CD3ζ complex; these cells thus function as reporter cells that become GFP-positive upon NKG2D ligation (36–38). THP1 cells were exposed to SADR-1 or SADR-2 for 48 h to allow surface expression of ULBP2 and were then co-cultivated with 2B4_NKG2D^{pos} or 2B4_NKG2D^{neg} cells. Monocytes exposed to SADR-1 induced a significantly stronger signal through NKG2D than cells exposed to SADR-2, whereas no GFP expression was observed in 2B4_NKG2D^{neg} control cells (Fig. 2*C*). Pretreatment of monocytes with a soluble NKG2D-Fc receptor completely abrogated the GFP expression, confirming that the activation was mediated by NKG2D (Fig. S2*A*). Expression of human NKG2D on 2B4_NKG2D^{pos} cells was confirmed (Fig. S2*B*), and specificity of ULBP2 interaction with NKG2D was confirmed by blocking ULBP2 prior to analysis of NKG2D-fc interaction (Fig. S2*C*).

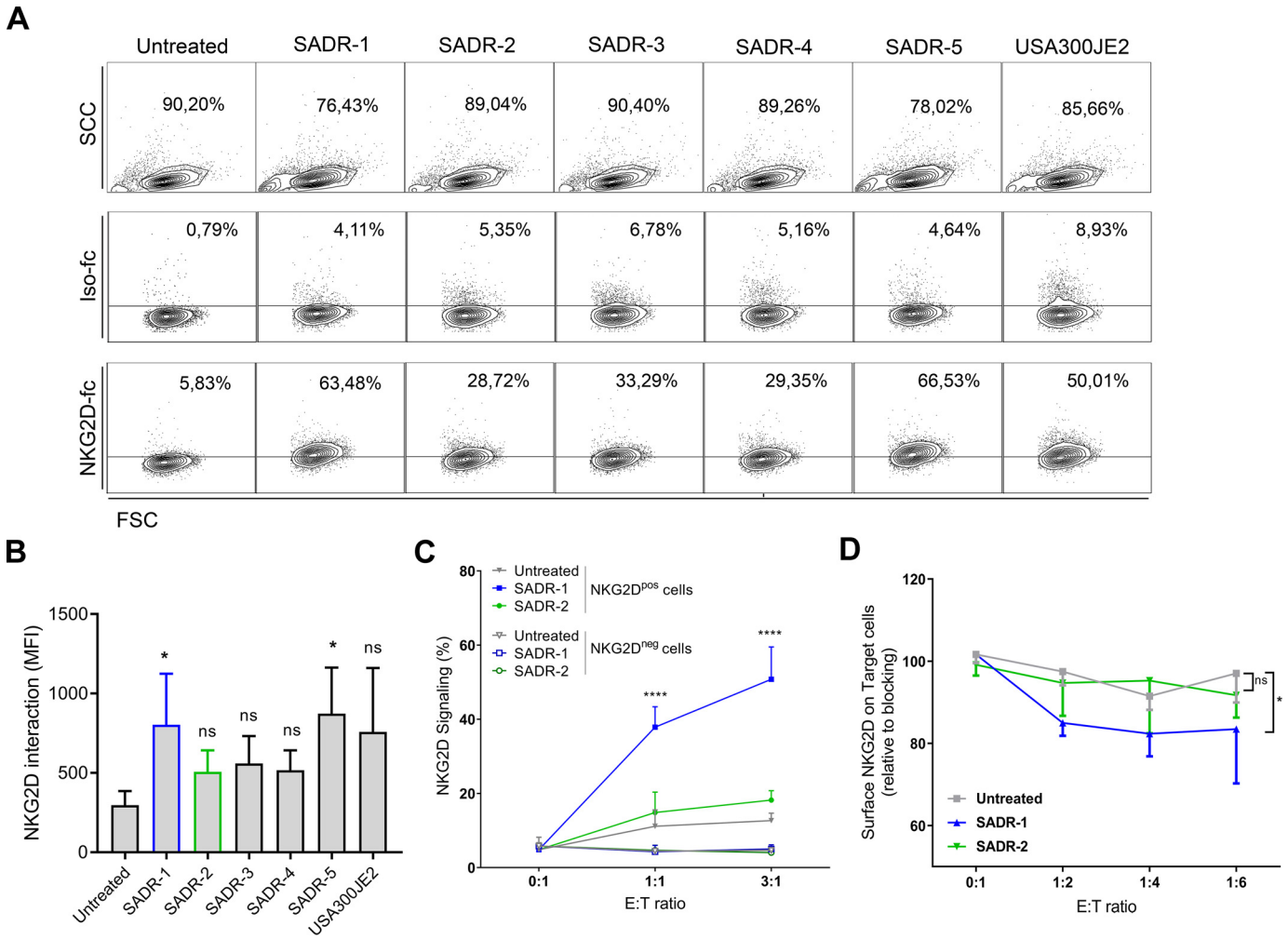

Figure 2. SADR-2 fails to induce NKG2D-mediated immune response compared with SADR-1. THP1 cells were treated with SADR-1–SADR-5 or USA300JE2. Functional ULBP2 expression was assessed by interaction with AF647-conjugated NKG2D-Fc after 48 h by flow cytometry, presented as follows: *A*, dot plots showing forward–side scatter and percentage gated cells (*top row*), percentage Iso-fc surface interaction (*middle row*), and NKG2D-Fc surface interaction (*bottom row*), representative for three independent experiments; and *B*, bar graph showing NKG2D-Fc surface interaction as MFI of data from three independent experiments. *C*, NKG2D signaling was assessed by co-cultivation of effector cells (THP1 cells) with target cells (2B4_NKG2D^{neg} or 2B4_NKG2D^{pos} cells) at the indicated effector–target (*E:T*) ratios for 14–16 h prior to analysis by flow cytometry. Before co-cultivation effector cells were treated with SADR-1 or SADR-2 for 48 h, and target cells were labeled with the membrane dye DID. Signaling through the NKG2D receptor upon interaction with ULBP2 was assessed as GFP expression by flowcytometry. Graph depicts percentage GFP expression from three independent experiments. *D*, NKG2D down-modulation was assessed by co-cultivation of effector cells (THP1 cells) with target cells (NK/CD8$^+$ T cells) at the indicated effector–target (*E:T*) ratios for 2.5 h prior to analysis by flow cytometry. Prior to co-cultivation, effector cells were treated with SADR-1 or SADR-2 for 48 h and treated with NKG2D-Fc (to block NKG2D ligands) or IgG1-Fc (control). Surface expression of NKG2D on target cells was measured by flow cytometry. Graph depicts surface NKG2D expression relative to NKG2D blocking on target cells from three donors in independent experiments. Statistical analysis was performed by one-way ANOVA with Dunnett's multiple comparisons test for data in *B*, two-way ANOVA with Tukey's multiple comparisons test for data in *C*, and two-way ANOVA with Dunnett's multiple comparisons test for data in *D*. Statistics are presented relative to untreated control and SADR-2 in *C*. *SCC*, side scatter; *FSC*, forward scatter; *ns*, not significant.

Following ligand interaction, the NKG2D receptor is down-regulated from the cell surface (39–41). We therefore investigated NKG2D receptor expression on primary natural killer and CD8$^+$ T cells after co-cultivation with SADR-1– or SADR-2–pretreated monocytes. Prior to co-cultivation, monocytes were incubated with either soluble NKG2D-Fc or IgG1-Fc control. Consistent with the NKG2D signaling data, SADR-1 induced a more potent NKG2D down-modulation than SADR-2 for all tested Effector:Target (*E:T*) ratios (Fig. 2*D*). Collectively, these data show that SADR-1 induces a potent, functional NKG2D ligand response compared with SADR-2, highlighting that the immune stimulatory structures on SADR-1 facilitating ULBP2 expression are altered by the mutations in SADR-2.

SADR-2 accumulates intracellularly in human monocytes compared with SADR-1

Myeloid responses to bacteria are orchestrated by signals from surface receptors, as well as through phagocytosis and degradation (27, 42). Phagocytosis and intracellular degradation initiate inflammasome activation and secretion of mature IL-1β (43, 44). Because *S. aureus*–induced ULBP2 surface expression occurred relatively late after stimulation (Fig. 1*B*), we hypothesized that ULBP2 induction by *S. aureus* was linked to phagocytosis and degradation. We therefore investigated cellular localization of SADR-1 and SADR-2 in THP1 cells by confocal microscopy. This was done by labeling *S. aureus* isolates with Alexa Fluor 647–conjugated succinimidyl-ester (AF–SADR) prior to stimulating monocytes. After 48 h, both SADR-

1 (AF–SADR-1) and SADR-2 (AF–SADR-2) were observed inside the monocytes, with relatively more SADR-2 than SADR-1 being visible (Fig. 3*A*). Next, we used flow cytometry to quantify intracellular *S. aureus* and found that the percentage of intracellular AF–SADR-2 was substantially higher compared with AF–SADR-1 at 24 h and significantly increased at 48 h (Fig. 3, *B* and *C*). This was not an artifact of unequal labeling of SADR-1 and SADR-2, because analysis of labeled and unlabeled *S. aureus* confirmed staining of the entire bacterial populations (Fig. S3*A*). Internalization of *S. aureus* was confirmed by analyzing the cell culture medium for labeled *S. aureus* at 48 h after exposure. Few bacteria were detected extracellularly (Fig. S3*B*), suggesting that SADR-1 is internalized and steadily degraded by the monocytes, whereas SADR-2 is internalized but accumulates intracellularly. Finally, we assessed intracellular association of all *S. aureus* strains by flow cytometry, showing significant accumulation of AF–SADR-3, AF–SADR-4, and interestingly AF–USA300JE2, whereas AF–SADR-5 resembled AF–SADR-1 (Fig. 3*C*). Labeling of *S. aureus* and bacteria in cell culture medium was verified by flow cytometry (Fig. S3*C*).

SADR-2 is more resistant to lysozyme-mediated degradation compared with SADR-1

Alterations in the staphylococcal cell wall facilitated by antibiotic treatment can alter susceptibility to lysozyme and phagosomal degradation (45–47), leading to fewer bacterial cell wall components released intracellularly, thus reducing inflammatory signaling and immune activation (43, 44). We therefore examined whether exposure to daptomycin had rendered SADR-2 resistant to degradation by lysozyme, an integral phagolysosomal enzyme. We cultivated SADR-1 and SADR-2 in the presence of lysozyme and subsequently monitored *S. aureus* membrane integrity through bacterial density (A_{600}) measurements. The optical density of the SADR-1 culture dropped (a sign of cell lysis) following addition of lysozyme (Fig. 4*A*). The optical density of the SADR-2 culture remained stable, and after 24 h the difference in bacterial growth was significantly reduced for SADR-1 compared with SADR-2, indicating that the acquired mutations in SADR-2 have made this isolate less susceptible to lysozyme (Fig. 4*A*).

We next investigated whether the induction of ULBP2 was associated with phagosomal degradation of *S. aureus*. First, we blocked degradation using bafilomycin, a selective vacuolar proton pump inhibitor (48). Bafilomycin treatment resulted in significantly reduced ULBP2 transcription, which was more pronounced for cells exposed to SADR-1 than SADR-2 (Fig. 4*B*). Similarly, the specific lysozyme inhibitor TriNAg (43, 49, 50) significantly decreased ULBP2 transcription in monocytes exposed to SADR-1, whereas ULBP2 transcription was only slightly reduced in cells exposed to SADR-2 (Fig. 4*C*). Cellular viability after inhibitor stimulation for 24 h was verified by annexin V and PI stain (Fig. S4). Collectively, these data indicate that phagosomal degradation of *S. aureus* is required for induction of ULBP2 expression and that SADR-2 is more resistant to degradation by lysozyme than SADR-1.

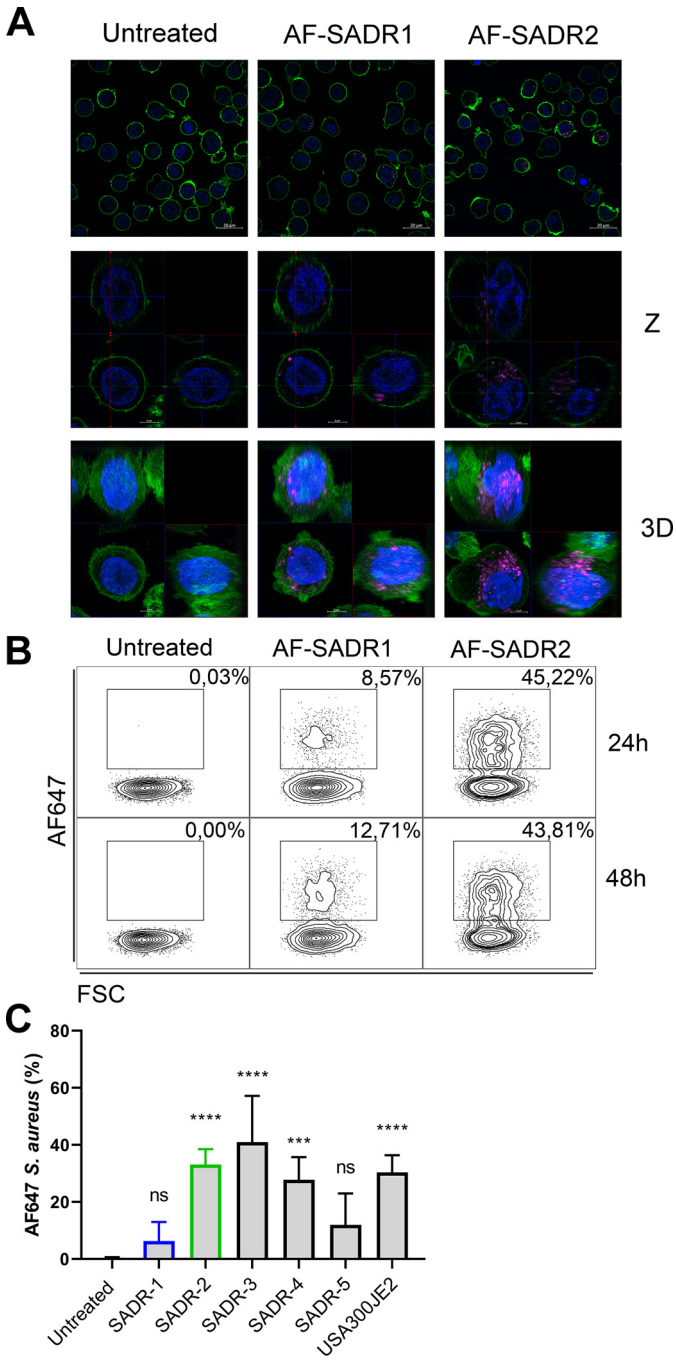

Figure 3. Increased intracellular pool of SADR-2 compared with SADR-1. *A*, THP1 cells were treated with AF647-labeled UV-SA (AF–SADR-1 or AF–SADR-2) for 48 h. Intracellular localization of labeled UV-SA was visualized by confocal microscopy. The cell surface was labeled with AF488-CD45 (*green*), and the nucleus was stained with Hoechst (*blue*) and AF647-labeled UV-SADR (*magenta*). The rows show overview of cells (*top row*), selected Z-plan projected as *x* axis *versus y* axis (*middle row*), and 3D structure presented as maximal intensity projection (*bottom row*). *B*, THP1 cells were treated with AF–SADR-1 or AF–SADR-2 for 24 or 48 h. Internalized bacteria were assessed by flow cytometry. Dot plots show percentage of internalized AF647-labeled UV-SA associated with viable THP1 cells. The data in *A* and *B* are representative of three independent experiments. *C*, THP1 cells were treated with AF–SADR-1–SADR-5 or AF–USA300JE2 for 48 h. Internalized bacteria were assessed by flow cytometry. Bar graph shows percentages of internalized AF647-labeled UV-SA associated with viable THP1 cells from three independent experiments. Statistical analysis was performed by one-way ANOVA with Dunnett's multiple comparisons test and presented relative to untreated control for data in *C*. *FSC*, forward scatter; *ns*, not significant.

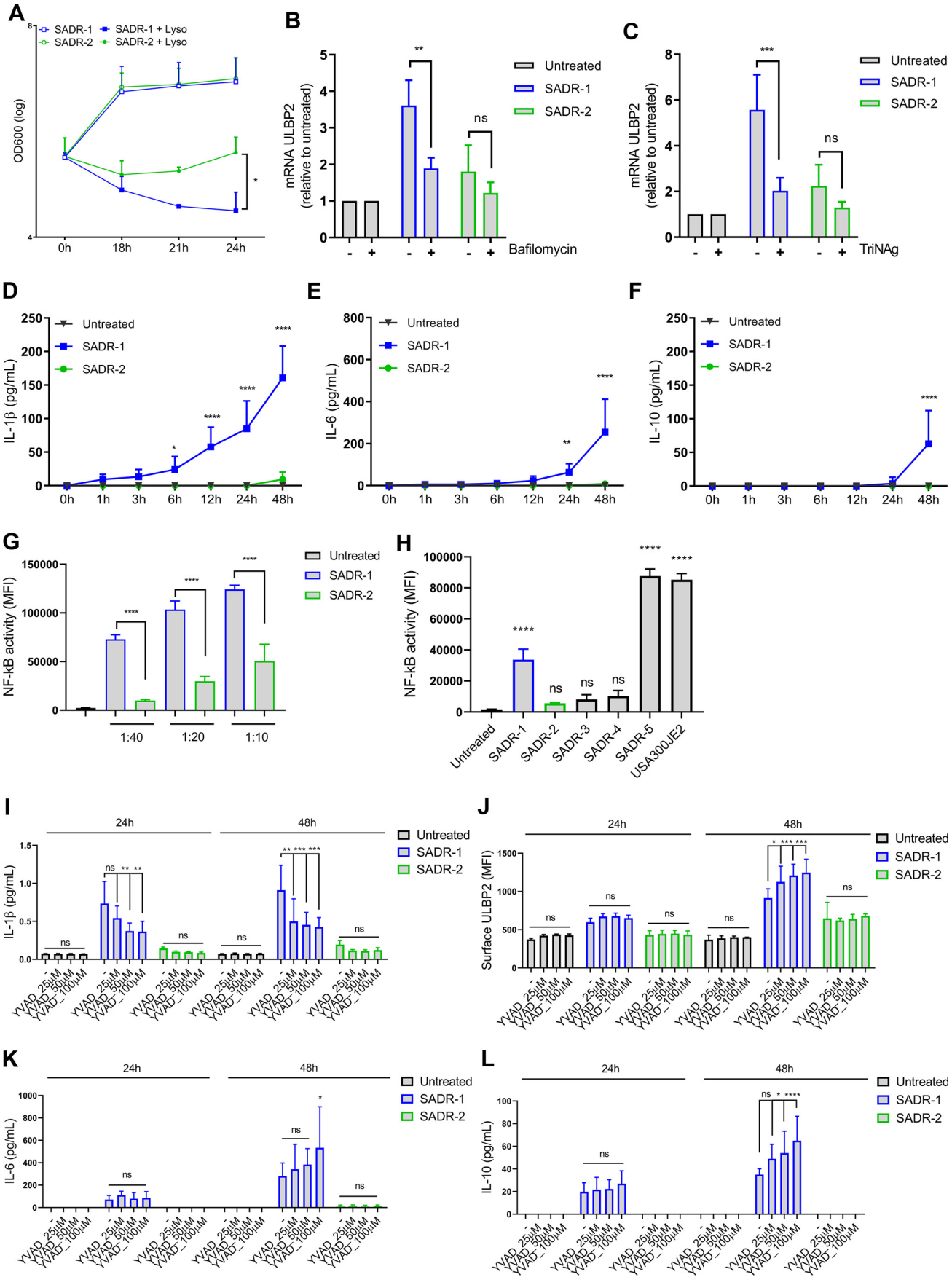
A
SADR-1
SADR-1 + Lyso
SADR-2
SADR-2 + Lyso
OD600 (log)
0h
18h
21h
24h
B
mRNA ULBP2 (relative to untreated)
Untreated
SADR-1
SADR-2
Bafilomycin
C
mRNA ULBP2 (relative to untreated)
Untreated
SADR-1
SADR-2
TriNAg
D
IL-1β (pg/mL)
Untreated
SADR-1
SADR-2
0h
1h
3h
6h
12h
24h
48h
E
IL-6 (pg/mL)
F
IL-10 (pg/mL)
G
NF-kB activity (MFI)
1:40
1:20
1:10
H
NF-kB activity (MFI)
Untreated
SADR-1
SADR-2
SADR-3
SADR-4
SADR-5
USA300JE2
I
IL-1β (pg/mL)
24h
48h
YVAD 25μM
YVAD 50μM
YVAD 100μM
J
Surface ULBP2 (MFI)
K
IL-6 (pg/mL)
L
IL-10 (pg/mL)

Stimulation of TLR2 on human monocytes can facilitate IL-6 and IL-10 release, whereas IL-1β secretion is linked to staphylococcal degradability (lysozyme sensitivity), release of inflammasome-activating components, and caspase 1 activity (18, 24, 25, 43, 47, 51). We therefore tested secretion of IL-1β, IL-6, and IL-10 in culture supernatants from monocytes exposed to SADR-1 or SADR-2. We found that only SADR-1 induced cytokine responses in the monocytes (Fig. 4, *D–F*). IL-1β secretion was rapidly induced and continued to increase during 48 h of stimulation (Fig. 4*D*), whereas secretion of IL-6 and IL-10 was initiated after 24 h (Fig. 4, *E* and *F*). These findings were supported by a significantly higher NF-κB activity in THP1–NF-κB–GFP reporter cells (52) responding to SADR-1 compared with SADR-2 (Fig. 4, *G* and *H*). Investigating NF-κB activity in response to all *S. aureus* isolates further revealed that SADR-3 and SADR-4 resembled SADR-2, whereas SADR-5 and USA300JE2 similar to SADR-1 increased activity significantly (Fig. 4*H*). NF-κB is important for production of pro–IL-β, whereas secretion of mature IL-1β depends on caspase 1 activity (43). To this end, we tested involvement of inflammasome activity on *S. aureus*–induced ULBP2 surface expression and cytokine secretion through treatment with the caspase 1 inhibitor, ac-YVAD-cmk (YVAD) (53). As expected, IL-1β secretion mediated by SADR-1 stimulation was significantly inhibited by YVAD (Fig. 4*I*). On the other hand, SADR-1–induced ULBP2 surface expression was significantly up-regulated by YVAD treatment for 48 h (Fig. 4*J*). This was in line with IL-6 (Fig. 4*K*) and IL-10 (Fig. 4*L*) secretion by SADR-1–stimulated cells, suggesting that ULBP2 surface expression is not dependent on inflammasome activation but is induced by a similar route as IL-6 and IL-10. Together, these data suggest that SADR-1 is more sensitive to degradation than SADR-2, resulting in higher immune activity of monocytes through both inflammasome-dependent (IL-1β) and -independent (ULBP2, IL-6, and IL-10) pathways.

Accumulation of intracellular (iso)citrate induces ULBP2 expression

Citrate is an integral tricarboxylic acid (TCA) cycle metabolite that is essential for supplying immune cells with energy and metabolites (54–56). Citrate is readily converted to its isomer, isocitrate, through aconitase activity (55). In phagocytic cells, (iso)citrate and derived molecules are important for the production of reactive oxygen species, NO, and prostaglandins making it a key metabolite in microbial immunity (57–60). In activated myeloid cells, induced activation of the citrate carrier is known to increase transport of (iso)citrate from mitochondria to the cytosol in exchange for malate (57, 59, 60). Lipopolysaccharide and *S. aureus* cause intracellular citrate increase in macrophages that results in inflammasome activation and IL-1β secretion (44).

We examined (iso)citrate accumulation in SADR-1– and SADR-2–stimulated cells after 6 and 12 h. Interestingly, isocitrate levels were significantly elevated in SADR-1–exposed cells compared with SADR-2–treated or untreated cells (Fig. 5*A*), whereas citrate was unaffected by either treatment (Fig. 5*B*). (Iso)citrate can be converted to the antibacterial compound itaconic acid (61, 62). However, we observed no accumulation of itaconic acid by SADR-1 or SADR-2 exposure (Fig. 5*C*).

To investigate a potential link between (iso)citrate buildup and ULBP2 expression, we treated monocytes with citrate alone or combined with SADR-1. We observed that citrate induced surface expression of ULBP2, and this effect was not additive with SADR-1 exposure (Fig. 5*D*), implying that SADR-1 and citrate induce ULBP2 through a similar signaling pathway. In agreement with this, both citrate and SADR-1 increased ULBP2 transcript levels (Fig. 5*E*). Interestingly, the citrate-mediated ULBP2 gene transcription occurred more rapidly than observed for SADR-1–exposed cells (Fig. 5*E*). The citrate analog hydroxycitrate (HC), has previously been used to inhibit the action of citrate (63, 64). In line with this, HC significantly inhibited SADR-1–mediated ULBP2 surface expression (Fig. 5*F*). Integrity and viability of the cells was verified by PI stain (Fig. S5). Together, these data indicate that the SADR-1–mediated (iso)citrate accumulation is linked to degradation of SADR-1, altered intracellular metabolism, and ULBP2 expression.

Inhibition of the glycolytic flow increases ULBP2 expression

Breakdown of *S. aureus* in phagosomes results in PGN degradation and release of intracellular GlcNAc, which induces a potent IL-1β response in lipopolysaccharide-primed macrophages (44). Because ULBP2 induction correlated with the ability to degrade *S. aureus*, we speculated whether GlcNAc released from *S. aureus* associated with ULBP2 expression. We found that GlcNAc treatment induced cell-surface expression of ULBP2 to some extent (Fig. 6*A* and Fig. S6*A*).

Cytoplasmic GlcNAc was shown to interact specifically with hexokinase, an essential enzyme in the glycolytic pathway

Figure 4. SADR-2 is more resistant to lysozyme-mediated degradation compared with SADR-1. *A*, SADR-1 and SADR-2 were grown to early stationary phase. The bacterial culture were then divided and mixed with either 300 μg/ml lysozyme or TSB as a control (0 h). Bacterial density was assessed by A_{600} measurement after 18, 21, and 24 h. The graphs show measurements from three independent experiments. *B*, THP1 cells were treated with SADR-1 or SADR-2, alone or combined with bafilomycin (50 nM). Total RNA was purified after 24 h and analyzed for ULBP2 expression by quantitative real-time PCR. Bar graphs in *B* and *C* show data from three independent experiments presented as fold change ± S.D. of ULBP2 mRNA normalized to the HKG and relative to the untreated, bafilomycin, or TriNAg controls. *C*, THP1 cells were treated with SADR-1 or SADR-2 alone or combined with TriNAg (0.5 mg/ml). Total RNA was purified after 24 h and analyzed for ULBP2 expression by quantitative real-time PCR. *D* and *F*, THP1 cells were treated with SADR-1 or SADR-2 for 48 h. Cytokines were measured in culture supernatants by ELISA at 1, 3, 6, 12, 24, and 48 h. Graphs show concentrations of secreted cytokines in supernatants from three independent experiments in IL-1β (*D*), IL-6 (*E*), and IL-10 (*F*). *G* and *H*, THP1–NF-κB–GFP reporter cells were treated with indicated concentrations of SADR-1 or SADR-2 for 24 h in *G* and SADR-1–SADR-5 or USA300JE2 (1:20) in *H*. NF-κB activity was assessed as GFP expression by flow cytometry. Graphs depict MFI of GFP expression from three independent experiments as fold change ± S.D. *I–L*, THP1 cells were treated with SADR-1 or SADR-2 for 24 and 48 h alone or in combination with YVAD (25, 50, or 100 μM). Concentration of cytokines were measured in culture supernatants by ELISA in *I*, *K*, and *L* and ULBP2 surface expression by flow cytometry presented as MFI in *J*. Graphs show data collected from three independent experiments IL-1β (*I*), surface ULBP2 (*J*), IL-6 (*K*), and IL-10 (*L*). Statistical analysis was performed by two-way ANOVA with Tukey's multiple comparisons test for data in *A–G* and *I–L*, and one-way ANOVA with Dunnett's multiple comparisons test for data in *H*. Statistics are presented relative to untreated control and SADR-2 in *D–F*, relative to untreated in *H*, and relative to mock-treated (–) in *I–L*. *ns*, not significant.

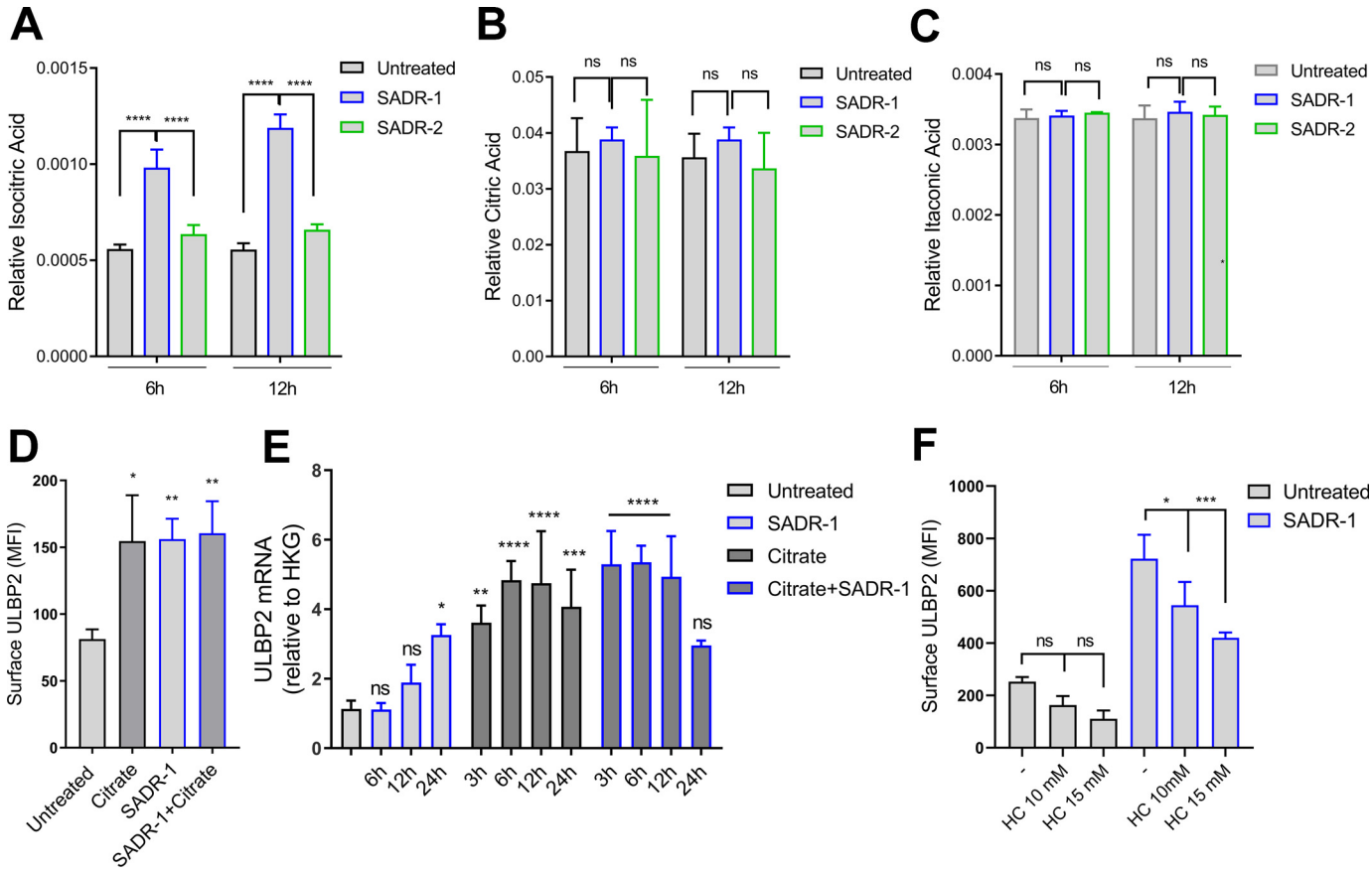

Figure 5. Accumulation of intracellular citrate induces ULBP2 expression. *A–C*, THP1 cells were treated with SADR-1 or SADR-2 for 6 or 12 h. Intracellular metabolites were extracted and analyzed by GC-MS. Bar graphs show relative values of metabolites from three independent experiments, in isocitrate (*A*), citrate (*B*), and itaconate (*C*). *D*, THP1 cells were treated with SADR-1 alone or combined with citrate (10 mM). Surface expression of ULBP2 was analyzed after 24 h by flow cytometry. Bar graph shows surface expression as MFI ± S.D. of data from three independent experiments. *E*, THP1 cells were treated with SADR-1, citrate (10 mM), or combined SADR-1 and citrate. Total RNA was purified after 3, 6, 12, and 24 h and analyzed for ULBP2 expression by quantitative real-time PCR. Bar graph shows data from three independent experiments, presented as fold change ± S.D. of ULBP2 mRNA normalized to the HKG. *F*, THP1 cells were treated with SADR-1 alone or combined with HC (10 or 15 mM). Surface expression of ULBP2 was analyzed after 48 h by flow cytometry. Bar graph shows surface expression as MFI ± S.D. of data from three independent experiments. Statistical analysis was performed by two-way ANOVA with Tukey's multiple comparisons test for data in *A–C* and *F*, one-way ANOVA with Tukey's multiple comparisons test for data in *D*, and two-way ANOVA with Dunnett's multiple comparisons test for data in *E*. Statistics are presented relative to untreated control in *D* and *E* and relative to untreated or SADR-1 (−) in *F*. Note that untreated and SADR-1–treated (6, 12, and 24 h) samples in *E* are also presented as controls in Fig. 6*C* (because citrate and 2DG treatment were performed in the same assay). *ns*, not significant.

resulting in reduced glycolytic flow (44). Furthermore, accumulated cytosolic citrate blocks the glycolytic pathway by inhibiting phosphofructokinase (44, 65). This prompted us to investigate ULBP2 expression in response to the glycolytic inhibitor 2-deoxy-D-glucose (2DG) (15, 66). Similar to citrate treatment, 2DG significantly induced ULBP2 expression (Fig. 6*B*). In addition, combined treatment of 2DG and *S. aureus* resulted in higher ULBP2 expression compared with *S. aureus* exposure alone (Fig. 6*B*). For SADR-2–SADR-4, addition of 2DG increased ULBP2 induction to a level similar to SADR-1, SADR-5, and USA300JE2 (Fig. 6*B*). 2DG also blocks the *N*-glycosylation pathway, which we have previously shown is important for surface expression of the NKG2D ligand MICA (15, 16, 66). Addition of D-mannose rescues the inhibition of *N*-glycosylation by 2DG (15). We confirmed by D-mannose treatment that altered *N*-glycosylation was not causing the regulatory effect on ULBP2 expression by 2DG (Fig. S6*B*). Similar to *S. aureus*–mediated ULBP2 regulation, 2DG was found to increase ULBP2 by increased gene transcription (Fig. 6*C*). Like citrate, 2DG treatment induced ULBP2 mRNA more rapidly than SADR-1 (Figs. 5*E* and 6*C*). These data suggest that the immediate effect of glycolytic inhibition is related to ULBP2 expression, and this mechanism is delayed in *S. aureus*–exposed cells because of the initial need for phagocytosis and degradation.

S. aureus reduces glycolysis in human monocytes

Glycolysis and mitochondrial oxidative phosphorylation are important for the proinflammatory cytokine response mediated by TLR2 stimulation in myeloid cells, and mitochondrial activity seems essential for phagocytosis and bacterial degradation (67, 68). Given that ULBP2 expression associates with staphylococcal degradability and is induced by direct inhibition of glycolysis, *e.g.* by increased intracellular GlcNAc or citrate treatment, it is likely that *S. aureus* phagocytosis and degradation ultimately impairs glycolysis. We assessed the glycolytic flow and capacity in monocytes after exposure to SADR-1 or SADR-2 by performing a glycolytic stress test using Seahorse extracellular flux analysis. The cells were glucose-starved for 1 h before glucose was added to measure the current reliance of

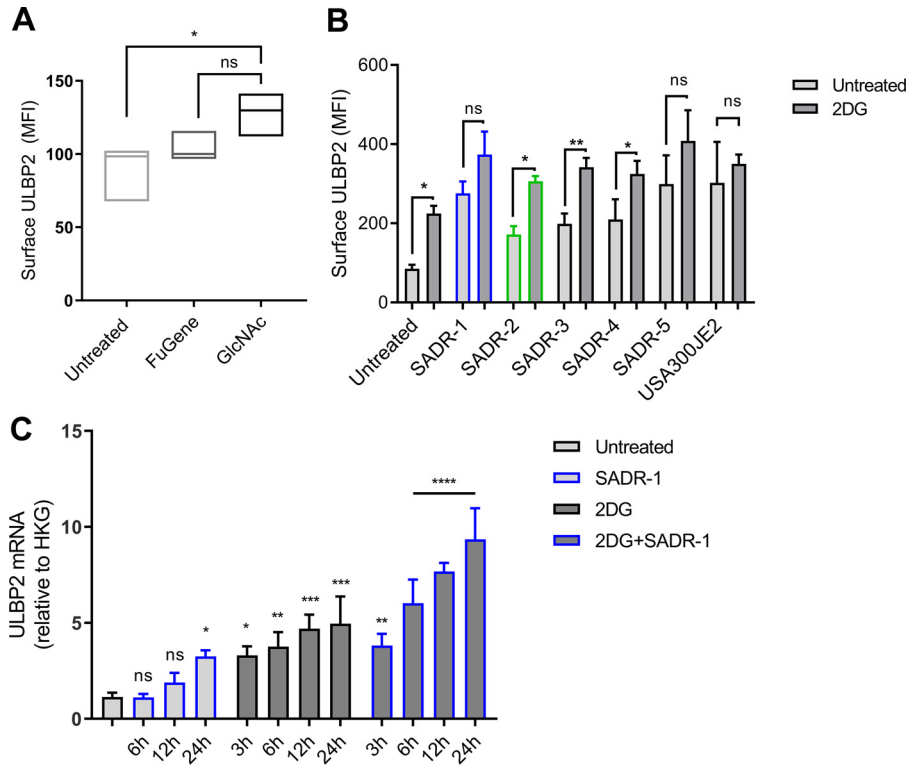

Figure 6. Inhibition of the glycolytic flow increases ULBP2 expression. *A*, THP1 cells were treated with FuGENE-complexed GlcNAc (*GlcNAc*), FuGENE alone (*FuGene*), or PBS (*Untreated*). Surface expression of ULBP2 was analyzed after 24 h by flow cytometry. *B*, THP1 cells were treated with indicated UV-SA, 2DG (10 mM), or combined UV-SA and 2DG. Surface expression of ULBP2 was analyzed after 48 h by flow cytometry. *C*, THP1 cells were treated with SADR-1, 2DG (10 mM), or combined SADR-1 and 2DG. Total RNA was purified after 3, 6, 12, and 24 h and analyzed for ULBP2 expression by quantitative real-time PCR. Bar graph shows data from three independent experiments, presented as fold change ± S.D. of ULBP2 mRNA normalized to the HKG. Data in *A* and *B* show surface expression as MFI ± S.D. of data from three independent experiments. Statistical analysis was performed by one-way ANOVA with Tukey's multiple comparisons test for data in *A*, two-way ANOVA with Sidaks's multiple comparisons test for data presented in *B*, and two-way ANOVA with Dunnett's multiple comparisons test for data presented in *C*. Statistics are presented relative to untreated control in *C*. Note that untreated and SADR-1–treated (6, 12, and 24 h) samples in *C* are also presented as controls in Fig. 5*E* (because citrate and 2DG treatment were performed in the same assay). *ns*, not significant.

glycolysis. We observed a decrease in glycolysis in SADR-1– or SADR-2–exposed cells compared with untreated cells at 24 h (Fig. 7, *A* and *B*). Furthermore, the glycolytic capacity and glycolytic reserve were increased in response to SADR-1 treatment (Fig. 7, *A* and *B*). In agreement with previous findings (67), this shows an increased capacity in *S. aureus*–stimulated cells to utilize glycolysis when mitochondrial activity is blocked (by addition of oligomycin). In contrast SADR-2 only slightly induced the glycolytic capacity (Fig. 7*B*).

To investigate glucose metabolism in *S. aureus*–exposed monocytes, we exposed cells to SADR-1 or SADR-2 in the presence of ^{13}C-labeled glucose. The results showed a significant reduction in labeling of central metabolites in both the first and second turns of the TCA cycle upon stimulation with SADR-1 compared with untreated or SADR-2–stimulated cells (Fig. 7, *C* and *D*). A similar although less pronounced labeling pattern was observed after 12 h (Fig. S7, *A* and *B*). The glycolytic contribution to the TCA cycle is therefore decreased after SADR-1 exposure. To study the effect of SADR-1 and SADR-2 on aerobic glycolysis, we measured intracellular lactate levels and saw a significant reduction in intracellular lactate levels after 24 h (Fig. 7*E*). The metabolic tracing studies are thus in line with the observed reduced glycolysis after SADR-1 exposure.

S. aureus–induced ULBP2 depends on functional mitochondria

To maintain ATP production, the cells can adapt to inhibited glycolysis by increasing mitochondrial activity (69). Because SADR-1 induced ULBP2 in a manner similar to glycolytic inhibitors, we examined whether ULBP2 induction by SADR-1 depended on functional mitochondria. Uncoupling the mitochondrial membrane potential with the ionophore, FCCP resulted in inhibition of ULBP2 by SADR-1 (Fig. 7*F*). We further tested etomoxir, an inhibitor of mitochondrial fatty acid import (CPT1a inhibitor), which was recently shown to act as a general inhibitor of mitochondrial function (70). Similar to FCCP, etomoxir impaired SADR-1–induced ULBP2 expression (Fig. 7*G*). Cellular viability was verified by PI stain after 48 h of incubation with FCCP (Fig. S7*D*) or etomoxir (Fig. S7*E*). Together, this suggests that SADR-1 promotes ULBP2 expression in monocytes in a mitochondrial-dependent manner.

Collectively, these data indicate that SADR-1 activates monocyte expression of ULBP2 after bacterial phagocytosis and degradation, which inhibits glycolysis and thereby promotes mitochondrial-dependent ULBP2 expression. On the other hand, SADR-2 is less degradable, releasing low amounts of intracellular signaling molecules, and hence accumulates silently intracellularly.

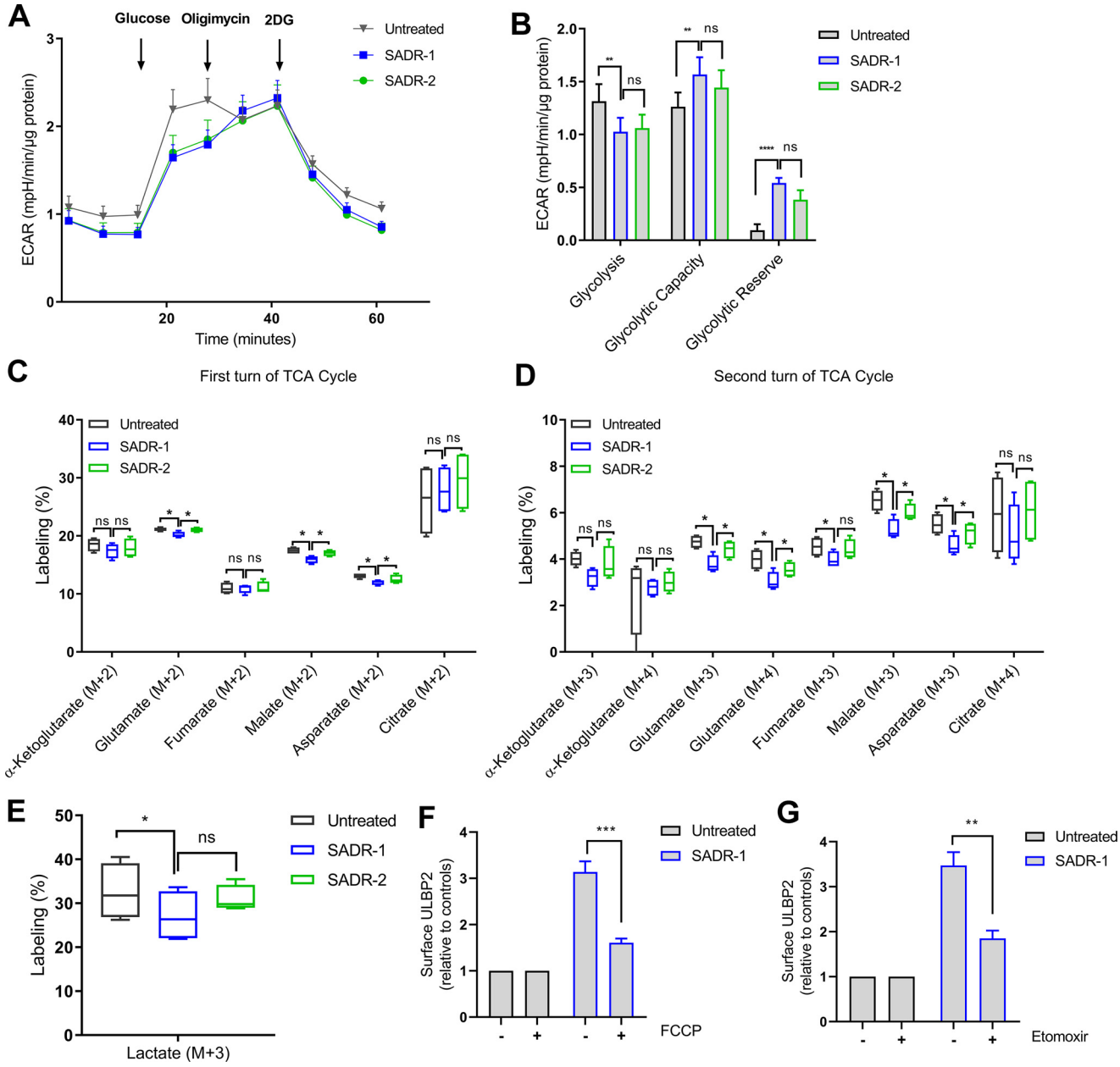

Figure 7. *S. aureus*–induced ULBP2 depends on functional mitochondria and inhibited glycolysis. *A* and *B*, THP1 cells were treated with SADR-1 or SADR-2. Glycolytic stress test was measured by Seahorse analysis after 24 h. The data are presented as the fluctuation in ECAR (*A*) and the glycolytic capacity, glycolytic reserve, and glycolysis measured presented as ECAR normalized to protein content (*B*, described in detail in "Materials and methods"). *C–E*, THP1 cells were treated with SADR-1 or SADR-2 in medium containing ^{13}C-labeled glucose. The processing of labeled glucose was analyzed by GC-MS to determine the percentage of ^{13}C distribution in intracellular metabolites. The data are presented as percentages of ^{13}C-labeled metabolite (described in detail in "Materials and methods") for ^{13}C incorporation in key TCA cycle metabolites after 24 h from the first turn in the cycle (*C*), from the second turn (*D*), and ^{13}C incorporation in intracellular lactate (*E*). *F*, THP1 cells were treated with SADR-1 alone or combined with FCCP (2,5 μM). Surface expression of ULBP2 was analyzed after 48 h by flow cytometry. *G*, THP1 cells were treated with SADR-1 alone or combined with etomoxir (400 μM). Surface expression of ULBP2 was analyzed after 48 h by flow cytometry. *A* and *B* show ECAR ± S.E. from eight independent experiments. *C–E* show percentages of ^{13}C labeling ± S.E. from four independent experiments. Bar graphs in *F* and *G* show data from three independent experiments presented as fold change ± S.D. of ULBP2 surface expression relative to the untreated, FCCP, or etomoxir controls. Statistical analysis was performed by two-way ANOVA with Tukey's multiple comparisons test for data in *B–E*, and unpaired two-tailed *t test* in *F* and *G*. *ns*, not significant.

Reversion of clpP in SADR-2 restores its immune stimulatory phenotype

To determine whether the hampered immune stimulatory phenotype of SADR-2 compared with SADR-1 was related to the SNPs in *rpoB* and/or *clpP*, four new *S. aureus* isolates were generated. First, the mutant *clpP* allele present in SADR-2 was reverted to the WT *clpP* in SADR-1. Two biological independent clones confirmed not to harbor unrelated secondary mutations were selected for further analysis (SADR-2^{clpP_rev_A} and SADR-2^{clpP_rev_B}). Second, the mutant alleles of *rpoB* and *clpP* present in SADR-2 were separately introduced in SADR-1 (SADR-1^{rpoB_mut} and SADR-1^{clpP_mut}). Of note, SADR-1^{rpoB_mut}

was a clean mutant, whereas SADR-1^{clpP_mut} carried two missense mutations in oleate hydratase and endonuclease mut S2 in addition to the *clpP* mutation.

We investigated ULBP2 mRNA and surface expression in THP1 cells after stimulation with the new *S. aureus* isolates. Interestingly, we found that SADR-2 with the reverted *clpP* (SADR-2^{clpP_rev_A} and SADR-2^{clpP_rev_B}) similar to SADR-1 significantly up-regulated ULBP2 on the surface (Fig. 8, *A* and *B*) and mRNA level in THP1 cells (Fig. 8*C*). Moreover, introducing the *clpP* mutation in SADR-1 (SADR-1^{clpP_mut}) did not induce ULBP2, whereas the *rpoB* mutation in SADR-1 (SADR-1^{rpoB_mut}) had no influence on the ability of SADR-1 to increase ULBP2 expression (Fig. 8, *A–C*). Finally, no other NKG2D ligands than ULBP2 were induced on the THP1 cell surface in response to either *S. aureus* isolate (Fig. S8*A*).

To assess the functional outcome of the *clpP* and *rpoB* mutations on monocyte immune activity, we investigated NKG2D receptor interaction by the *S. aureus*-regulated ULBP2. We found an interaction pattern of the NKG2D receptor similar to the ULBP2 expression pattern, showing that SADR-1, SADR-2^{clpP_rev_A}, and SADR-2^{clpP_rev_B}, and SADR-1^{rpoB_mut} significantly increased NKG2D interaction compared with SADR-2 and SADR-1^{clpP_mut} (Fig. 8, *A* and *D*).

We previously found that SADR-2, compared with SADR-1, accumulated intracellularly and did not activate NF-κB activity (Figs. 3, *A–C*, and 4, *G* and *H*). We therefore tested accumulation and NF-κB activity in response to the new isolates using THP1 and THP1–NF-κB–GFP reporter cells, respectively. Interestingly, reversion of *clpP* in SADR-2 significantly decreased bacteria associated with viable THP1 cells (intracellular bacteria), whereas introduction of *clpP* mutation in SADR-1 significantly increased accumulation compared with SADR-1 carrying the *rpoB* mutation (Fig. 8*E*). Proper labeling and bacteria in culture supernatants were confirmed by flow cytometry (Fig. S8*B*). In addition, we found that in line with SADR-1, SADR-2^{clpP_rev_A}, SADR-2^{clpP_rev_B}, and SADR-1^{rpoB_mut} significantly increased NF-κB activity compared with SADR-2 and SADR-1^{clpP_mut} (Fig. 8, *F* and *G*). Finally, we tested secretion of IL-1β, IL-6, and IL-10 after *S. aureus* stimulation at 48 h. Also here, the reversion of *clpP* in SADR-2 (SADR-2^{clpP_rev_A} and SADR-2^{clpP_rev_B}) stimulated cytokine secretion similar to SADR-1 and SADR-1^{rpoB_mut} (Fig. 8, *H–J*), whereas SADR-1^{clpP_mut} in line with SADR-2 did not stimulate cytokine secretion by THP1 cells (Fig. 8, *H–J*).

Discussion

We show that NKG2D ligands are induced in human monocytes in response to *S. aureus*. We demonstrate that ULBP2 expression is mediated through enhanced gene expression related to intracellular degradation of *S. aureus*. Degradation of *S. aureus* and increased cytoplasmic (iso)citrate associates with ULBP2 expression. Furthermore, our results suggest that SADR-1–induced ULBP2 is linked to a shift in the intracellular metabolism from glycolysis to mitochondrial oxidation. Regulation of NKG2D ligands have been coupled to DNA damage and reactive oxygen species production often mediated by external stressors (9, 12, 71), but it has not previously been linked to an immune-metabolic mechanism in human monocytes. Previous studies have associated TLR signaling with NKG2D ligand expression on human monocytes and exposure to *S. aureus* in mouse macrophages (40, 72, 73). Our data suggest that ULBP2 is induced through an inflammasome-independent pathway. We furthermore show that *S. aureus*–mediated ULBP2 expression in THP1 cells is abrogated by *clpP* mutation but not *rpoB*.

Exposure to antibiotics can alter cell wall structure and intracellular degradation of *S. aureus* that potentiates and directs the immune response (43, 44, 47, 74, 75). We found that SADR-2 was more resistant to lysozyme-mediated degradation than SADR-1. SADR-2 has a structurally altered cell wall compared with SADR-1, likely because of the mutations in *rpoB* and *clpP* causing reduced daptomycin susceptibility and virulence (30). Lysozyme targets PGN (46), and pathogenic *S. aureus* can modify their PGN structure via *O*-acetylation through *O*-acetylase A (OatA), activity making the bacteria resistant to lysozyme (45, 46). Daptomycin exposure has not previously been linked to alterations in PGN. However, the stress regulator Spx that is up-regulated in SADR-2–SADR-4 is important for regulating OatA activity in other Gram-positive bacteria (30, 76), indicating a possible link between daptomycin-mediated cell wall alterations and lysozyme sensitivity via OatA activity.

GlcNAc is one of the main components in the cross-linked network of carbohydrates present in bacterial PGN and is released upon intracellular degradation of *S. aureus* (28). When investigating the direct influence of GlcNAc on ULBP2 expression, we observed a modest induction of ULBP2. This is likely explained by a limited cellular uptake of GlcNAc even when complexed with transfecting agent or prolonged exposure to increase cytosolic delivery, as previously described (44). An important effect of cytosolic GlcNAc is inhibition of glycolysis (44, 77). Likewise, we found that the glucose analog 2DG, which is efficiently taken up via glucose transporters and blocks the glycolytic pathway (15, 66), significantly increased ULBP2 transcript and surface expression.

When investigating metabolic activity in the monocytes responding to *S. aureus*, we found that in particular SADR-1 reduced glycolysis but increased the cellular glycolytic capacity, the latter likely induced by an early (surface interaction–induced) glycolytic activity, corresponding with intracellular lactate levels at 12 h (Fig. S7*C*) and previous findings (67). In addition the intracellular isocitrate levels were increased after SADR-1 exposure, and there was no apparent increase in citrate levels. In other studies we have found that the intracellular citrate concentration is strongly regulated, so increased citrate production can mainly be measured by increased flux and not by increased concentration.[8] Anyway, citrate is likely involved in ULBP2 expression because it significantly induced ULBP2. In support of this, the citrate inhibitor hydroxycitrate potently inhibited SADR-1–induced ULBP2. Citrate is also an effective inhibitor of glycolysis (44, 65), and we hypothesize that the combined action of intracellular released GlcNAc and citrate causes the observed reduced glycolysis and

[8] Møller S. H., Mellergaard M., Madsen M., Bermejo A. V., Jepsen S. D., Hansen M. H., Høgh R. I., et al, submitted for publication.

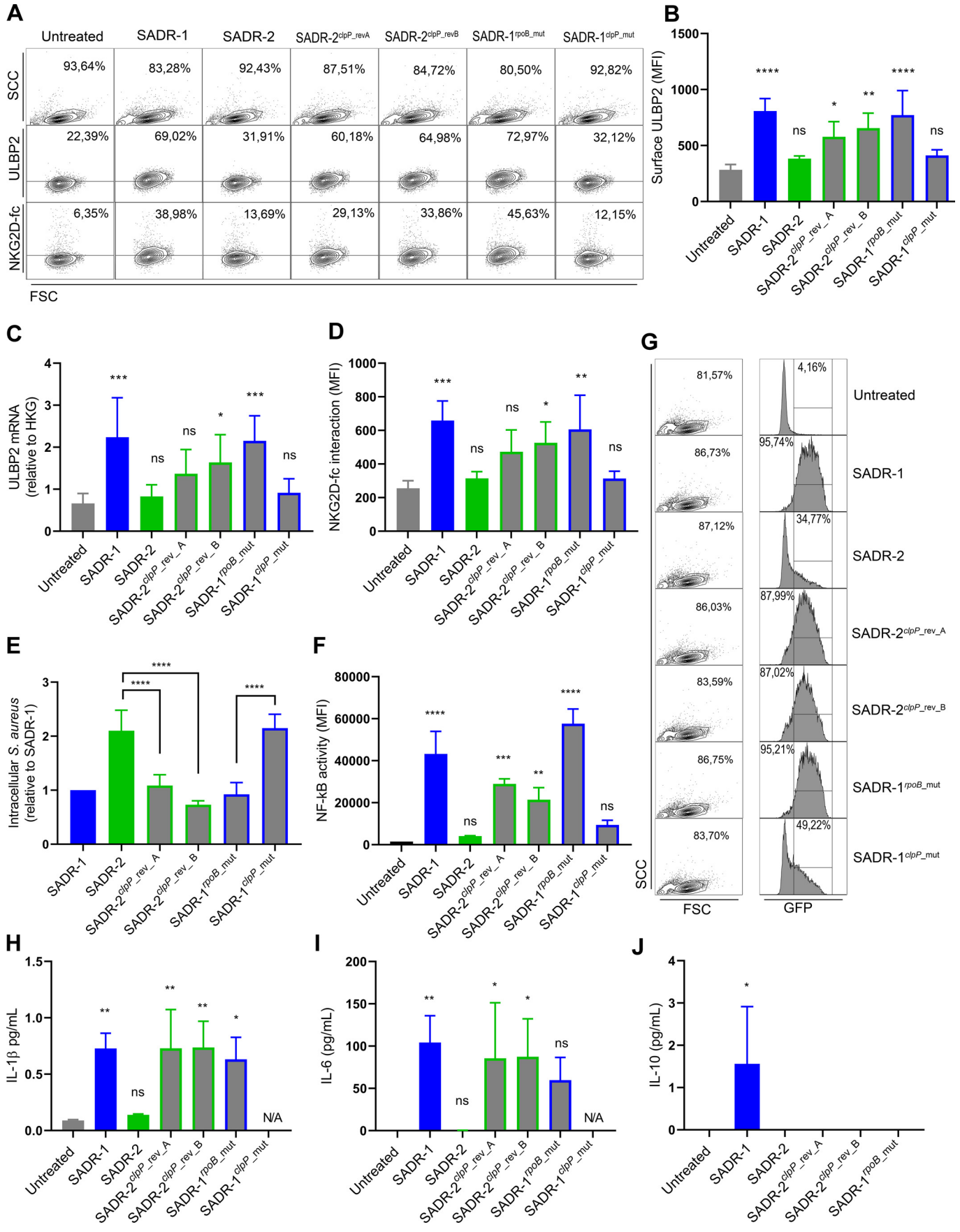
A
Untreated
SADR-1
SADR-2
SADR-2clpP_revA
SADR-2clpP_revB
SADR-1rpoB_mut
SADR-1clpP_mut
SCC
ULBP2
NKG2D-fc
93,64%
83,28%
92,43%
87,51%
84,72%
80,50%
92,82%
22,39%
69,02%
31,91%
60,18%
64,98%
72,97%
32,12%
6,35%
38,98%
13,69%
29,13%
33,86%
45,63%
12,15%
FSC
B
Surface ULBP2 (MFI)
C
ULBP2 mRNA (relative to HKG)
D
NKG2D-fc interaction (MFI)
E
Intracellular S. aureus (relative to SADR-1)
F
NF-kB activity (MFI)
G
81,57%
86,73%
87,12%
86,03%
83,59%
86,75%
83,70%
4,16%
95,74%
34,77%
87,99%
87,02%
95,21%
49,22%
SCC
FSC
GFP
H
IL-1β pg/mL
I
IL-6 (pg/mL)
J
IL-10 (pg/mL)
ns
N/A

SADR-1–induced ULBP2. Cellular metabolism is a constant balance between glycolytic and mitochondrial activity. To this end, hampered glycolysis will result in an increased reliance on mitochondrial activity, necessary for bacterial killing and ULBP2 expression. Recent studies showed that mitochondrial activity is linked to staphylococcal degradation and killing in human monocytes (67, 68).

SADR-2 was selected *in vivo* and differs from SADR-1 by only two single SNPs in the *rpoB* and *clpP* genes that are linked to daptomycin susceptibility and staphylococcal stress control and virulence, respectively (6, 30, 33, 34). However, it is not clear how these mutations influence immunity to *S. aureus* (30, 78). Our data indicate that *clpP* but not *rpoB* hampers human monocytic immunity to SADR-2, suggesting a new immune evasive mechanism of *S. aureus.* It has been suggested that phagolysosomal resistant *S. aureus* accumulate silently intracellularly because of the absence of released inflammatory signals (29). We show that both SADR-1 and SADR-2 are recognized and internalized by human monocytes. However, SADR-1 induced NF-κB activity, IL-1β, IL-6, and IL-10, as well as a robust ULBP2 response, whereas significantly lower NF-κB, nearly no cytokine, and nonfunctional ULBP2 induction was detected in response to SADR-2. Surface recognition primes cells for production of pro–IL-1β, whereas intracellular inflammasome activity is necessary for secretion of mature IL-1β (27, 79). Our results suggest that resistant SADR-2 does not fully activate either the surface or intracellular inflammatory signaling cascade necessary for NF-κB activity, cytokine secretion, or ULBP2 induction and thereby accumulates silently in human monocytes.

SADR-2–SADR-4 are likely all less sensitive to degradation because of vital alterations in structural features of their cell wall, possibly mediated by an abrogated *clpP–clpX* pathway and increased Spx activity (30, 35, 76), seemingly making these strains able to silently persist inside human monocytes. SADR-5 is highly interesting because this isolate also carries the *rpoB* A477D mutation, but in contrast to SADR-2–SADR-4, SADR-5 induces NF-κB activity and ULBP2 on the surface of THP1 cells, further supporting our findings that the *clpP* mutation and likely hampered *clpP–clpX* pathway in SADR-2 are essential for the increased resistance to lysozyme observed in this isolate. Involvement of the *clpX* and the *clpP–clpX* pathway, as well as intracellular degradability and accumulation, however, requires further experimental verification. Together, these findings highlight that NKG2D-mediated immunity is activated upon staphylococcal infections through an inflammasome-independent and imposed inflammatory shift in the intracellular metabolism of the phagocytosing monocytes, thus defining a target for future anti-staphylococcal therapy that can be used against persistent *S. aureus* infections.

Materials and methods

Human cells and culture conditions

The human acute monocytic leukemia cell line (THP1) was purchased from the American Type Culture Collection. THP1–NF-κB–GFP reporter cells were kindly provided by Dr. Peter Steinberger (Institute of Immunology, Medical University of Vienna, Vienna, Austria). 2B4_NKG2D^{neg} and 2B4_NKG2D^{pos} T-cell hybridoma cell lines were kindly provided by Dr. Chiwen Chang (Department of Pathology, University of Cambridge, Cambridge, United Kingdom). The 2B4 (2B4_NKG2D^{neg}) and CT312 (2B4_NKG2D^{pos}) cells were previously described (36–38). The cells were cultivated in RPMI 1640 (Sigma, R5886) supplemented with 10% FBS (Sigma, F9665), 2 mM L-glutamine (Sigma, G7513), 2 mM penicillin and streptomycin (Sigma, P4333), as previously described (80), unless otherwise specified. Primary monocytes were isolated by EasySep human monocyte enrichment kit (Stem Cell, Vancouver, Canada, 15068) and cultivated in standard RPMI medium further supplemented with macrophage colony–stimulating factor (Prepotech, 300-25) for 2–3 days.

Bacterial strains and culture conditions

SADR-1 (A9781), SADR-2 (A9788), SADR-3 (A9784), SADR-4 (A9792), and SADR-5 (A9798) were previously described (original names in parentheses) (6, 30). The USA300 strain JE2 was purchased from the Network of Antimicrobial Resistance in *S. aureus* Program. SADR-2^{clpP_rev_A}, SADR-2^{clpP_rev_B} (two different clones of SADR-2 with reverted *clpP*-D94G), SADR-1^{rpoB_mut}, and SADR-1^{clpP_mut} (SADR-1 with introduced mutations in *rpoB*-A477D and *clpP*-G94D, respectively) were prepared in this study (described below). Strains were cultivated in TSB (tryptic soy broth medium; Oxoid, Hampshire, UK, CM0129B) at 200 rpm and at 37 °C with TSA (Oxoid, CM0131B). Growth conditions were as previously described (6, 30). Lysozyme assay was performed as previously

Figure 8. *ClpP* reversion restores the immunogenic phenotype in SADR-2. *A–D*, THP1 cells were treated with SADR-1, SADR-2, and SADR-2 with reverted clpP (SADR-2^{clpP_rev_A} or SADR-2^{clpP_rev_B}), SADR-1 with an introduced rpoB (SADR-1^{rpoB_mut}), or clpP (SADR-1^{clpP_mut}) mutation. mRNA purification was done after 24 h, and flow cytometry analysis was performed after 48 h. The data are presented as follows: *A*, dot plots showing forward–side scatter and percentage gated cells (*top row*), percentage ULBP2 surface expression (*middle row*), and percentage NKG2D-Fc surface interaction (*bottom row*), representative for three independent experiments; *B*, bar graph showing ULBP2 surface expression; *C*, bar graph showing ULBP2 mRNA relative to HKG; *D*, bar graph showing NKG2D-fc surface interaction; and *E*, THP1 cells were treated with AF–SADR-1, AF–SADR-2, AF–SADR-2^{clpP_rev_A}, AF–SADR-2^{clpP_rev_B}, AF–SADR-1^{rpoB_mut}, or AF–SADR-1^{clpP_mut} for 48 h. Internalized bacteria were assessed by flow cytometry. Bar graphs show percentage of internalized AF647-labeled UV-SA relative to AF–SADR-1, associated with viable THP1 cells from five independent experiments. *F* and *G*, THP1–NF-κB–GFP reporter cells were treated with SADR-1, SADR-2, SADR-2^{clpP_rev_A}, SADR-2^{clpP_rev_B}, SADR-1^{rpoB_mut}, or SADR-1^{clpP_mut} (1:20) for 24 h. NF-κB activity was assessed as GFP expression by flow cytometry. *F*, graphs depict MFI of GFP expression from three independent experiments as fold change ± S.D. G, histograms show gating in forward–side scatter plots (*left column*) and percentage GFP expression (*right column*) representative of three independent experiments. *H–J*, THP1 cells were treated with SADR-1, SADR-2, SADR-2^{clpP_rev_A}, SADR-2^{clpP_rev_B}, SADR-1^{rpoB_mut}, or SADR-1^{clpP_mut} for 48 h. Cytokines were measured in culture supernatants by ELISA. Graphs show concentration of secreted cytokines in supernatants from three independent experiments in IL-1β (*H*), IL-6 (*I*), and IL-10 (*J*). Graph depicts data from three independent experiments as MFI ± S.D. for flow cytometry data in *B*, *D*, and *F*; fold change ± S.D. of ULBP2 mRNA normalized to the HKG ± S.D. in *C*; fold change ± S.D. intracellular *S. aureus* for five independent experiments in *E*; cytokine concentration ± S.D. for ELISA data in *H–J*. Statistical analysis was performed by one-way ANOVA with Dunnett's multiple comparisons test and presented relative to untreated control for data in *B–D*, *F*, and *H–J*; and one-way ANOVA with Tukey's multiple comparisons test for data in *E*. *SCC*, side scatter; *FSC*, forward scatter; *ns*, not significant.

described (46); in brief *S. aureus* strains were grown in Erlenmeyer flasks to the early stationary phase (A_{600} = 5–6). Bacterial cultures were split in two new flasks, and to one was added 300 μg/ml lysozyme (Roche, Basel, Switzerland, 10837059001); A_{600} was measured after 18, 21, and 24 h.

Sequencing bacterial strains

Whole genome sequencing (WGS) was performed on SADR-1 and SADR-2 by isolating genomic DNA from overnight culture in brain–heart infusion (BHI) broth (Oxoid) with the DNeasy blood and tissue kit (Qiagen). Before DNA extraction, harvested cells were treated with lysostaphin (Ambi), added to the Gram-positive lysis buffer (final concentration 100 μg/ml), and incubated at 37 °C for 30 min. WGS was performed on an Illumina NextSeq platform using Nextera XT libraries (150-bp paired ends) according to the manufacturer's instructions. SNP/indel calling were performed using the Snippy Pipeline version 3.0 and using SADR-1 and SADR-2 genomes assembled with skesa (81) as references. Potential structural variants were investigated by comparing the coverage of all reads, split reads, or discordant reads of SADR-1 and SADR-2 strains aligned onto the SADR-1 genome assembly. Sequencing reads were mapped with bwa mem v0.7.17-r1188 (82). Split and discordant mapped reads were extracted from the bam alignment files using the extractSplitReads_BwaMem script and the samtools command "samtools view -b -F 1294," respectively. The different bam alignment files of the different strains were then compared using Artemis software (83) to identify potential structural variants.

WGS revealed that SADR-2 harbors a G281A (G94D) mutation in *clpP* that was not reported in previous studies (6, 30). To test for the presence of the *clpP* mutation in SADR-1–SADR-5, the *clpP* gene was PCR-amplified using primers: 5′-GATAGGTGGCTATCAAGCG-3′ and 5′-CGAGTCAGCTAGTGGTCCG-3′ (purchased from Eurofins MWG Operon). The Qiagen purified PCR products were sequenced at Eurofins MWG Operon using primer 5′-AATTCCTACAGTTATGA-3′. Analysis of the sequences was performed using the free software CLC sequence viewer, version 8.0.

Construction of rpoB and clpP mutants by allelic exchange

Allelic exchange experiments were performed using shuttle vector pIMAY-Z (84) and using the method described in Ref. 85 with minor modifications. Full-length *rpoB* and *clpP* sequences corresponding to the SADR-1 and SADR-2 alleles were obtained by performing PCR with Phusion High-Fidelity DNA polymerase (New England Biolabs) and primer pairs pIM_rpobF/R and pIM_clpP_F/R. Gel-purified amplicons were then ligated to pIMAY-Z plasmid using seamless ligation cloning extract (SLiCE) cloning (86) and transformed into *Escherichia coli* strain IM08B (84). The presence of a cloned insert was confirmed by colony PCR using primers pIM_MCS_F and pIM_MCS_R. Purified plasmids were then electroporated into *S. aureus* strains SADR-1 or SADR-2, and the transformations were plated onto BHI agar plates supplemented with chloramphenicol (Cm) at 10 mg/liter and X-gal (Melford) at 100 mg/l. The plates were incubated 48 h at 30 °C; the blue colonies were then picked and grown in BHI broth at 37 °C without Cm selection pressure overnight to allow the loss of the pIMAY-Z thermosensitive plasmid. White colonies with double cross-overs leading to allelic replacement were isolated directly onto X-gal BHI plates (introduction of *clpP*-D94G mutation into SADR-2) or BHI plated supplemented with 1 mg/liter of rifampicin (introduction of *rpoB*-A477D into SADR-1) or supplemented with 50 mg/liter of oxacillin (introduction of *clpP*-G94D into SADR-1). Clones were colony-purified onto BHI plates before glycerol storage and extraction of genomic DNA. To validate the allelic exchange procedure, the whole genome sequences of all reconstructed strains were determined with the Illumina Nextseq 500 sequencer and using Nextera XT paired-end libraries (2 × 150 bp reads). Sequencing reads of all mutant strains were mapped to SADR-1 and SADR-2 genomes using Snippy (version 4.6) to confirm the introduced mutations (https://github.com/tseemann/snippy). The primers used were as follows: pIM_rpob_F, CTCACTAAAGGGAACAAAAGCTGGGTACCTTGGCAGGTCAAGTTGTCCAATATG; pIM_rpob_R, CGACTCACTATAGGGCGAATTGGAGCTCTTAATCAGTAACTTCTTTTTGTGTTTCAGGAG; pIM_clpP_F, CCTCACTAAAGGGAACAAAAGCTGGGTACCATATTTCCGCTCAAAGTAT; pIM_clpP_R, CGACTCACTATAGGGCGAATTGGAGCTCTATCAGTTTACAAAGGAAAG; pIM-MCS_F, AATACCTGTGACGGAAGATCACTTCG; and pIM_MCS_R, TACATGTCAAGAATAAACTGCCAAAGC.

Preparation of live (live-SA) and UV-killed S. aureus (UV-SA)

S. aureus was inoculated from overnight TSA plates in fresh TSB to $A_{600} \sim 0{,}03$ and grown in Erlenmeyer flasks to the early stationary phase (A_{600} = 5–6 or 5–7 h of incubation). The bacteria were washed and resuspended in PBS to A_{600} = 1. Live-SA were added directly to cell cultures. For preparing UV-SA, 5 ml of live-SA was transferred to Petri dishes and subjected to pulsed UV radiation of 10.000 μJ/cm2 for 120 s (monochromatic wavelength of 254 nm; CL-1000 cross-linker; UVP, Cambridge, UK). Bacterial death was verified by plating on TSA plates and incubation at 37 °C overnight.

Stimulation of monocytes with S. aureus

Monocytes treated with UV-SA were seeded at 300,000 cells/ml, treated with 50 μl UV-SA/ml (THP1 cells) or 25 μl/ml (primary monocytes) cell suspension, and incubated at 37 °C with 5% CO_2 for 1–48 h. THP1 cells treated with live-SA were plated in RPMI 1640 medium supplemented with 10% FBS (Sigma, F9665), 2 mM L-glutamine (Sigma, G7513), and 10 μg/ml streptomycin (Sigma, S9137). The cells were stimulated with PBS as untreated control or UV-killed *S. aureus*, unless otherwise specified.

Flow cytometry

Cell-surface staining was done as previously described (80), with the exception that monocytes were blocked using FcR-blocking solution (Miltenyi Biotec, North Rhine, Westphalia, Germany, 120-000-442) prior to antibody staining. The antibodies used were ULBP2/5/6 (R&D Systems, FAB1298A), MICA/B (BD Biosciences, 558352), ULBP1

(R&D Systems, FAB1380P), ULBP3 (R&D Systems, FAB1517A), ULBP4 (R&D Systems, FAB6285A), ULBP2 (R&D Systems, MAB1298), mouse IgG2A (R&D Systems, MAB0031), anti-mouse IgG (Biolegend, 405308), annexin V (BD Biosciences, 640919), PI (Sigma, P4864), recombinant human NKG2D-Fc chimera (R&D Systems, 1299-NK) or recombinant human IgG1-Fc (R&D Systems, 110-HG), and Zenon Alexa Fluor 647 human IgG labeling kit (Molecular Probes, Z-25408). Isotype controls were from BD Biosciences. Analysis was done using an Accuri C6 flow cytometer, CFlow software, and FlowLogic version 700.2A (Inivai Technologies Pty, Australia). Gating was done on viable cells in forward–side scatter plots, and the grid was set according to isotype controls (5%, except for dot plots in Fig. 1*C*). Mean fluorescence intensity (MFI) values were presented as isotype MFI subtracted from MFI of specific staining.

Quantitative real-time PCR

mRNA was isolated from cells treated with *S. aureus* for 3–24 h using TRIzol reagent (Invitrogen, 15596026) and Direct-zol RNA Miniprep (Zymo Research, R2050S). mRNA was converted to cDNA by Quanta qScript cDNA SuperMix (Quanta Biosciences, 95048). The ribosomal protein, large P0 (RPLP0) was used as a housekeeping gene (HKG). The primer sequences for PCR were as follows: Forward_ RPLP0_119: 5′-CCT-CGTGGAAGTGACATCGT-3′; Reverse_ RPLP0_433, 5′-CATTCCCCCGGATATGAGGC-3′; Forward_ULBP2_ 378, 5′-CAGAG-CAACTGCGTGACATT-3′; and Reverse_ULBP2_610, 5′-GGCCACAACCTTG-TCATTCT-3′. The primers were purchased from Eurofins MWG Operon. PCR amplification was performed using SYBR Green master mix with low ROX (Quanta Biosciences, 95074 or QuantiNova, Qiagen, 208056) on an Agilent AriaMx apparatus, and analysis was done with Agilent Aria Mx (Agilent). Expression levels of NKG2D ligands were normalized to expression of the HKG, unless otherwise specified.

NKG2D signaling assay

Effector cells (THP1) were treated with UV-SA for 48 h before the cells were blocked with NKG2D-Fc (R&D Systems, 1299-NK) or control IgG1-Fc (R&D Systems, 110-HG) for 30 min at 4 °C. Target cells (2B4_NKG2D^{neg} and 2B4_NKG2D^{pos}) were stained with the Vybrant cell-labeling kit, color DID (1 μl/ml to 1×10^6 cells/ml) (Molecular Probes, V22889). Target and effector cells were mixed at the indicated ratios and co-cultured at 37 °C with 5% CO_2 for 14–16 h before analysis by flow cytometry.

NKG2D down-modulation assay

Peripheral blood mononuclear cells were isolated by Histopaque 1077 density gradient centrifugation (Sigma, 10771). Peripheral blood lymphocytes (PBLs) from these cells were purified by 1–2 h of incubation with Dynabeads (Invitrogen, 110.41). $CD4^+$ T cells were removed from PBLs by positive depletion of $CD4^+$ cells using CD4 antibody (eBioscience, 16-0049) and Dynabeads (Invitrogen, 110.41). $CD4^+$-depleted PBLs were cultivated in standard RPMI medium (described above) supplemented with 10% human serum (Sigma, H4522) and 10 ng/ml recombinant IL-15 (Prepotech) for 3 days, as previously described (41). Effector cells (THP1) were treated with UV-SA for 48 h, and the cells were blocked with NKG2D-Fc (R&D Systems, 1299-NK) or control IgG1-Fc (R&D Systems, 110-HG) for 30 min at 4 °C. Target cells ($CD4^+$-depleted PBLs) were added, and the cells were co-cultured for 2.5 h. NKG2D down-modulation was assessed on $CD4^+$-depleted PBLs blocked with IgG1-Fc relative to NKG2D-Fc blocking.

Seahorse glycolytic function analysis

Glycolytic capacity of THP1 cells was assessed by the Seahorse XFe96 extracellular flux analyzer (Seahorse Biosciences–Agilent Technologies) using the standard glycolysis stress test. THP1 cells were treated with UV-SA or PBS (untreated) and incubated at 37 °C with 5% CO_2 for 24 h. The cells were washed in unbuffered Dulbecco's modified Eagle's medium (Sigma, D5030) supplemented with 2 mM glutamine (Sigma, G3126), pH 7.4. The cells were equilibrated for 1 h at 37 °C in a CO_2-free incubator. The extracellular acidification rate (ECAR) measurement cycle consisted of 3 min of mixing and 3 min of measurement of acidification. Analysis was initiated by three baseline ECAR measurement cycles, followed by the sequential injection of glucose (10 mM, Sigma, 49159), oligomycin (1 μM, Sigma, 75351), and 2DG (50 mM, Sigma, D6134) with two ECAR measurement cycles in between each injection and three final measurement cycles. ECAR was recorded and calculated by the Seahorse XFe96 software, Wave. Subsequently the protein content was measured for each well using the Pierce BCA assay with BSA as standard. Based on the ECAR measurements, the glycolytic parameters were calculated as follows: (*a*) glycolysis (last measurement before glucose injection subtracted from last measurement before oligomycin injection), (*b*) glycolytic capacity (last measurement before glucose injection subtracted from last measurement before 2DG injection), and (*c*) glycolytic reserve (glycolysis subtracted from glycolytic capacity). The results are presented as mean values ± S.E. (87).

Metabolism of ^{13}C-labeled glucose

THP1 cells were incubated in medium containing uniformly labeled glucose ([U-^{13}C]glucose (99%) ^{13}C-enriched; CLM-1396-10, Cambridge Isotopes Laboratories Inc.). The cells were plated in unlabeled glucose-free RPMI 1640 medium (Gibco, 11879-020) with 10% FBS (Sigma, F9665), 2 mM L-glutamine (Sigma, G7513), 2 mM penicillin and streptomycin (Sigma, P4333), and enriched with 10 mM ([U-^{13}C]glucose), treated with UV-SA or PBS (untreated), and incubated at 37 °C with 5% CO_2 for 12 or 24 h. The cells were washed, extracted in 70% ethanol, and centrifuged at 20,000 × *g* for 20 min (4 °C) to separate the soluble extract from the insoluble components. Cell extracts were lyophilized and reconstituted in water for biochemical analyses. Protein content was determined in the dissolved pellets as previously described (87, 88). Extract samples were adjusted to pH 1–2 with HCl and evaporated to dryness under nitrogen flow. Analytes were extracted into an organic phase (96% ethanol/benzene) followed by derivatization with 14% N,N-dimethylformamide (DMF), 86% N-tert-butyldimethylsilyl-N-methyltrifluoroacetamide (MTBSTFA) with a modified procedure from (89). Standards containing

unlabeled metabolites of interest and cell extracts were separated and analyzed in a gas chromatograph (Agilent Technologies 7820A chromatograph, J&W GC column HP-5MS, parts no. 19091S-433) coupled to a mass spectrometer (Agilent Technologies, 5977E). The isotopic enrichment of the metabolites of interest was corrected for natural abundance of ^{13}C using the unlabeled standards and calculated according to Ref. 90. The data are presented as labeling (%) of $M + X$, where M is the mass of the unlabeled molecule, and X is the number of labeled C-atoms in a given metabolite (87).

Cytokine measurements

Cytokine levels in supernatants from THP1 cells treated with UV-SA were assessed at 1–48 h after treatment. Standard ELISA was used for measuring human IL-1β (R&D Systems, DY201), human IL-6 (R&D Systems, DY206) and human IL-10 (R&D Systems, DY217B). The samples were run on a BioTek PowerWave instrument and analyzed using KC4v3.0 software.

Metabolomics

Intracellular levels of metabolites from THP1 cells were analyzed by GC-MS. 3.6×10^6 THP1 cells were treated with UV-SA for 6 or 12 h. The cells were washed, flash-frozen in liquid nitrogen, and stored at −80 °C. Extraction of metabolites was performed as described in Ref. 91. In brief, metabolites were extracted by two snap freezes in methanol and one snap freeze in MilliQ water. The methanol and water extracts were pooled and dried under nitrogen flow before derivatized with methyl chloroformate to obtain volatile products. The samples were analyzed by GC-MS at MS-Omics Aps. Derivatization and analysis were performed using a slightly modified version of the protocol described in Ref. 92. A mixed pooled sample was made from small aliquots of each individual sample to ensure quality control. Raw GC-MS data were processed using the data software PARADISe described in Ref. 93.

Confocal microscopy and phagocytosis analysis

UV-SA strains were labeled with AF647-conjugated succinimidyl-ester (SE-AF647; Molecular Probes, A-20006). Bacteria were centrifuged at 10,000 × *g* 10 min 4 °C and resuspended in original volume of sodium bicarbonate buffer (pH 8.5). SE-AF647 was added in a final concentration of 9 ng/μl and bacteria were incubated at 4 °C for 1 h with agitation. Stained bacteria were washed and resuspended to original volume in PBS. THP1 cells were treated with stained UV-SA for 24–48 h. Human cells were washed twice in PBS with 2% FBS. For flow cytometry, the cells were analyzed directly, whereas for microscopy, they were stained with 1 μg/ml Hoechst 33342 (Thermo Scientific, 62249) at 37 °C for 15 min and stained with AF488-conjugated CD45 (Biolegend, 304019) at 4 °C for 30 min. Finally, the samples were washed and resuspended in 60 μl of PBS. Confocal images were taken using a Carl Zeiss LSM780 confocal system with a Plan-Apochromat 63×/1.4 oil-immersion objective. The 405-, 505-, and 633-nm lasers were used to excite Hoechst 33342, AF488-CD45, and SE-AF647, respectively. Fluorescent signals were collected using a fMBS 405/505c beam splitter and acquired in the same track to minimize cell movement during acquisition. Images were processed using the software Zen Blue version 2.3. Fluorescent signal from AF488-CD45 was subtracted from the Hoechst signal during image processing to allow for a separate nuclear signal.

GlcNAc treatment

Treatment of THP1 cells with GlcNAc was done by cultivating cells in standard RPMI further supplemented with GlcNAc (25 mM or 50 mM) for up to 3 weeks prior to UV-SA stimulation and analysis or with inspiration from Wolf *et al.* (44). GlcNAc (Sigma, catalog no. A3286) was dissolved in fresh Optimem (Gibco, 31985-062) to 1 M, pH ~7.4. 100 μl of GlcNAc solution was then mixed with 3 μl of FuGENE (Promega, Wisconsin, United States, E2313) and incubated for 1–1.5 h at room temperature. The FuGENE-complexed GlcNAc was added to cells (50 μl/ml) and incubated for 24 h at 37 °C with 5% CO_2.

Reagents

2-Deoxy D-Glucose (Sigma, D6134), sodium citrate (Sigma, 234265), bafilomycin (Sigma, SML1661), TriNAg (*N*,*N*′,*N*′′-triacetylchitotriose; Santa Cruz, sc-222016), ac-YVAD-cmk (Sigma, SML0429), FCCP (Sigma, C2920), etomoxir (Cayman Chemical, 828934-41-4), and hydroxycitrate (potassium hydroxycitrate tribasic monohydrate; Sigma, 59847).

Statistical analysis

Data preparation and statistical analysis were performed using the software GraphPad Prism, version 8.01 (GraphPad Software). Statistical analysis was performed and presented as stated in the figure legends, and the level of statistical significance was determined by a p value of <0.05 and presented as follows: *, $p < 0.05$; **, $p < 0.01$; ***, $p < 0.001$; and ****, $p < 0.0001$.

Ethics statement

Primary cells were isolated from buffy coats from healthy human volunteer donors, obtained from the State Hospital (Copenhagen, Denmark). Informed written consents were obtained from all donors in accordance with legislation and guidelines from the local ethics committee (Region Hovedstaden, Denmark).

Data availability

Supporting information accompanies this article online. Data will be shared upon request to the corresponding author, Søren Skov.

Acknowledgments—We thank Dr. Peter Steinberger (Institute of Immunology, Medical University of Vienna, Vienna, Austria) for THP1–NF-κB–GFP reporter cells and Dr. Chiwen Chang (Department of Pathology, University of Cambridge, Cambridge, UK) for providing 2B4 and 2B4_NKG2D cells. We acknowledge the Core Facility for Integrated Microscopy (Faculty of Health and Medical Sciences, University of Copenhagen, Denmark) for guidance in confocal microscopy imaging. We acknowledge MS-Omics Aps

(Frederiksberg, University of Copenhagen, Denmark) for metabolite analysis. We also thanks Anni Mehlsen (Department of Veterinary and Animal Sciences, University of Copenhagen, Copenhagen, Denmark) for invaluable technical assistance.

Author contributions—M. M., R. I. H., A. L., A. S. H., N. P., Z. F., S. D. J., C. H. F. H., L. A., A. R. L., A. Y. P., T. P. S., B. P. H., H. S. W., D. F., and S. S. conceptualization; M. M., R. I. H., A. Y. P., T. P. S., D. F., and S. S. formal analysis; M. M., L. A., and A. R. L. funding acquisition; M. M., R. I. H., A. L., B. I. A., R. G., S. H. M., A. S. H., S. D. J., and C. H. F. H. investigation; M. M., R. I. H., A. L., B. I. A., RG, S. H. M., A. S. H., N. P., Z. F., S. D. J., C. H. F. H., L. A., A. R. L., A. Y. P., B. P. H., H. S. W., D. F., and S. S. methodology; M. M., T. P. S., and S. S. writing-original draft; M. M. project administration; M. M., R. I. H., A. L., B. I. A., R. G., S. H. M., A. S. H., N. P., Z. F., S. D. J., C. H. F. H., L. A., A. R. L., A. Y. P., T. P. S., B. P. H., H. S. W., D. F., and S. S. writing-review and editing; R. I. H. data curation; L. A., A. R. L., A. Y. P., T. P. S., D. F., and S. S. supervision.

Funding and additional information—This work was supported by Ph.D. Scholarship A3507 from the University of Copenhagen Faculty of Health and Medical Sciences (to M. M.), Else and Mogens Wedell Wedellsborg Foundation Grant 3A-17-1 (to M. M.), Danish Council for Independent Research Grant DFF-6111-00499 (to S. S.), and Novo Nordisk Foundation Grant NNF15CC0018346 (to S. S.).

Conflict of interest—The authors declare that they have no conflicts of interest with the contents of this article.

Abbreviations—The abbreviations used are: MRSA, methicillin-resistant *S. aureus*; TLR, Toll-like receptor; PGN, peptidoglycan; IL, interleukin; SNP, single-nucleotide polymorphism; AF, Alexa Fluor 647–conjugated; TCA, tricarboxylic acid; HC, hydroxycitrate; PI, propidium iodide; 2DG, 2-deoxy-d-glucose; FCCP, ionophore trifluoromethoxy carbonylcyanide phenylhydrazone; FBS, fetal bovine serum; TSA, tryptic soy agar; WGS, whole genome sequencing; BHI, brain–heart infusion; X-gal, 5-bromo-4-chloro-3-indolyl β-d-galactoside; live-SA, live *S. aureus*; UV-SA, UV-killed *S. aureus*; MFI, mean fluorescence intensity; HKG, housekeeping gene; PBL, peripheral blood lymphocyte; ECAR, extracellular acidification rate; SE-AF647, AF647-conjugated succinimidyl-ester; ANOVA, analysis of variance.

References

1. Tong, S. Y., Davis, J. S., Eichenberger, E., Holland, T. L., and Fowler, V. G., Jr. (2015) *Staphylococcus aureus* infections: epidemiology, pathophysiology, clinical manifestations, and management. *Clin. Microbiol. Rev.* **28,** 603–661 CrossRef Medline
2. Lowy, F. D. (2003) Antimicrobial resistance: the example of *Staphylococcus aureus*. *J. Clin. Invest.* **111,** 1265–1273 CrossRef Medline
3. Chambers, H. F., and DeLeo, F. R. (2009) Waves of resistance: *Staphylococcus aureus* in the antibiotic era. *Nat. Rev. Microbiol.* **7,** 629–641 CrossRef Medline
4. Bayer, A. S., Schneider, T., and Sahl, H.-G. (2013) Mechanisms of daptomycin resistance in *Staphylococcus aureus*: role of the cell membrane and cell wall. *Ann. N. Y. Acad. Sci.* **1277,** 139–158 CrossRef Medline
5. Gould, I. M., David, M. Z., Esposito, S., Garau, J., Lina, G., Mazzei, T., and Peters, G. (2012) New insights into meticillin-resistant *Staphylococcus aureus* (MRSA) pathogenesis, treatment and resistance. *Int. J. Antimicrob. Agents* **39,** 96–104 CrossRef Medline
6. Peleg, A. Y., Miyakis, S., Ward, D. V., Earl, A. M., Rubio, A., Cameron, D. R., Pillai, S., Moellering, R. C., Jr., and Eliopoulos, G. M. (2012) Whole genome characterization of the mechanisms of daptomycin resistance in clinical and laboratory derived isolates of *Staphylococcus aureus*. *PLoS One* **7,** e28316 CrossRef Medline
7. Stojanovic, A., Correia, M. P., and Cerwenka, A. (2018) The NKG2D/NKG2DL axis in the crosstalk between lymphoid and myeloid cells in health and disease. *Front. Immunol.* **9,** 827 CrossRef Medline
8. Zhang, J., Basher, F., and Wu, J. D. (2015) NKG2D ligands in tumor immunity: two sides of a coin. *Front. Immunol.* **6,** 97 CrossRef Medline
9. Champsaur, M., and Lanier, L. L. (2010) Effect of NKG2D ligand expression on host immune responses. *Immunol. Rev.* **235,** 267–285 CrossRef Medline
10. Eagle, R. A. A., and T, J. (2007) Promiscuity and the single receptor: NKG2D. *Nat. Rev. Immunol.* **7,** 737–744 CrossRef Medline
11. Carapito, R., and Bahram, S. (2015) Genetics, genomics, and evolutionary biology of NKG2D ligands. *Immunol. Rev.* **267,** 88–116 CrossRef Medline
12. Raulet, D. H., Gasser, S., Gowen, B. G., Deng, W., and Jung, H. (2013) Regulation of ligands for the NKG2D activating receptor. *Annu. Rev. Immunol.* **31,** 413–441 CrossRef Medline
13. Raffaghello, L., Prigione, I., Airoldi, I., Camoriano, M., Levreri, I., Gambini, C., Pende, D., Steinle, A., Ferrone, S., and Pistoia, V. (2004) Downregulation and/or release of NKG2D ligands as immune evasion strategy of human neuroblastoma. *Neoplasia* **6,** 558–568 CrossRef Medline
14. Groh, V., Wu, J., Yee, C., and Spies, T. (2002) Tumour-derived soluble MIC ligands impair expression of NKG2D and T-cell activation. *Nature* **419,** 734–738 CrossRef Medline
15. Andresen, L., Skovbakke, S. L., Persson, G., Hagemann-Jensen, M., Hansen, K. A., Jensen, H., and Skov, S. (2012) 2-deoxy D-glucose prevents cell surface expression of NKG2D ligands through inhibition of *N*-linked glycosylation. *J. Immunol.* **188,** 1847–1855 CrossRef Medline
16. Mellergaard, M., Skovbakke, S. L., Schneider, C. L., Lauridsen, F., Andresen, L., Jensen, H., and Skov, S. (2014) *N*-Glycosylation of asparagine 8 regulates surface expression of major histocompatibility complex class I chain-related protein A (MICA) alleles dependent on threonine 24. *J. Biol. Chem.* **289,** 20078–20091 CrossRef Medline
17. Serbina, N. V., Jia, T., Hohl, T. M., and Pamer, E. G. (2008) Monocyte-mediated defense against microbial pathogens. *Annu. Rev. Immunol.* **26,** 421–452 CrossRef Medline
18. Wong, K. L., Yeap, W. H., Tai, J. J., Ong, S. M., Dang, T. M., and Wong, S. C. (2012) The three human monocyte subsets: implications for health and disease. *Immunol. Res.* **53,** 41–57 CrossRef Medline
19. van Furth, R., Leijh, P. C., van Zwet, T. L., and van den Barselaar, M. T. (1982) Phagocytosis and intracellular killing by peripheral blood monocytes of patients with monocytic leukemia. *Blood* **59,** 1234–1238 CrossRef Medline
20. Hanzelmann, D., Joo, H. S., Franz-Wachtel, M., Hertlein, T., Stevanovic, S., Macek, B., Wolz, C., Götz, F., Otto, M., Kretschmer, D., and Peschel, A. (2016) Toll-like receptor 2 activation depends on lipopeptide shedding by bacterial surfactants. *Nat. Commun.* **7,** 12304 CrossRef Medline
21. Zheng, L., Zomerdijk, T. P., Aarnoudse, C., van Furth, R., and Nibbering, P. H. (1995) Role of protein kinase C isozymes in Fcγ receptor-mediated intracellular killing of *Staphylococcus aureus* by human monocytes. *J. Immunol.* **155,** 776–784 Medline
22. Zheng, L., Nibbering, P. H., and van Furth, R. (1992) Cytosolic free calcium is essential for immunoglobulin G–stimulated intracellular killing of *Staphylococcus aureus* by human monocytes. *Infect. Immun.* **60,** 3092–3097 CrossRef Medline
23. Wang, Z. M., Liu, C., and Dziarski, R. (2000) Chemokines are the main proinflammatory mediators in human monocytes activated by *Staphylococcus aureus*, peptidoglycan, and endotoxin. *J. Biol. Chem.* **275,** 20260–20267 CrossRef Medline
24. Chau, T. A., McCully, M. L., Brintnell, W., An, G., Kasper, K. J., Vinés, E. D., Kubes, P., Haeryfar, S. M., McCormick, J. K., Cairns, E., Heinrichs, D. E., and Madrenas, J. (2009) Toll-like receptor 2 ligands on the staphylococcal cell wall downregulate superantigen-induced T cell activation and prevent toxic shock syndrome. *Nat. Med.* **15,** 641–648 CrossRef Medline
25. Frodermann, V., Chau, T. A., Sayedyahossein, S., Toth, J. M., Heinrichs, D. E., and Madrenas, J. (2011) A modulatory interleukin-10 response to staphylococcal peptidoglycan prevents Th1/Th17 adaptive immunity to *Staphylococcus aureus*. *J. Infect. Dis.* **204,** 253–262 CrossRef Medline

26. Elson, G., Dunn-Siegrist, I., Daubeuf, B., and Pugin, J. (2007) Contribution of Toll-like receptors to the innate immune response to Gram-negative and Gram-positive bacteria. *Blood* **109,** 1574–1583 CrossRef Medline
27. Storek, K. M., and Monack, D. M. (2015) Bacterial recognition pathways that lead to inflammasome activation. *Immunol. Rev.* **265,** 112–129 CrossRef Medline
28. Davis, K. M., and Weiser, J. N. (2011) Modifications to the peptidoglycan backbone help bacteria to establish infection. *Infect. Immun.* **79,** 562–570 CrossRef Medline
29. Wolf, A. J., Liu, G. Y., and Underhill, D. M. (2017) Inflammatory properties of antibiotic-treated bacteria. *J. Leukoc. Biol.* **101,** 127–134 CrossRef Medline
30. Bæk, K. T., Thøgersen, L., Mogenssen, R. G., Mellergaard, M., Thomsen, L. E., Petersen, A., Skov, S., Cameron, D. R., Peleg, A. Y., and Frees, D. (2015) Stepwise decrease in daptomycin susceptibility in clinical *Staphylococcus aureus* isolates associated with an initial mutation in rpoB and a compensatory inactivation of the clpX gene. *Antimicrob. Agents Chemother.* **59,** 6983–6991 CrossRef Medline
31. Eagle, R. A., Traherne, J. A., Ashiru, O., Wills, M. R., and Trowsdale, J. (2006) Regulation of NKG2D ligand gene expression. *Hum. Immunol.* **67,** 159–169 CrossRef Medline
32. Nowbakht, P., Ionescu, M. C., Rohner, A., Kalberer, C. P., Rossy, E., Mori, L., Cosman, D., De Libero, G., and Wodnar-Filipowicz, A. (2005) Ligands for natural killer cell-activating receptors are expressed upon the maturation of normal myelomonocytic cells but at low levels in acute myeloid leukemias. *Blood* **105,** 3615–3622 CrossRef Medline
33. Guérillot, R., Gonçalves da Silva, A., Monk, I., Giulieri, S., Tomita, T., Alison, E., Porter, J., Pidot, S., Gao, W., Peleg, A. Y., Seemann, T., Stinear, T. P., and Howden, B. P. (2018) Convergent evolution driven by rifampin exacerbates the global burden of drug-resistant *Staphylococcus aureus*. *mSphere* **3,** e00550-17 CrossRef Medline
34. Lee, J. Y. H., Monk, I. R., Gonçalves da Silva, A., Seemann, T., Chua, K. Y. L., Kearns, A., Hill, R., Woodford, N., Bartels, M. D., Strommenger, B., Laurent, F., Dodémont, M., Deplano, A., Patel, R., Larsen, A. R., *et al.* (2018) Global spread of three multidrug-resistant lineages of *Staphylococcus epidermidis*. *Nat. Microbiol.* **3,** 1175–1185 CrossRef Medline
35. Frees, D., Brøndsted, L., and Ingmer, H. (2013) Bacterial proteases and virulence. In *Regulated Proteolysis in Microorganisms* (Dougan, D. A., ed) pp. 161–192, Springer, New York
36. Arase, H., Mocarski, E. S., Campbell, A. E., Hill, A. B., and Lanier, L. L. (2002) Direct recognition of cytomegalovirus by activating and inhibitory NK cell receptors. *Science* **296,** 1323–1326 CrossRef Medline
37. Andersson, A. K., Sumariwalla, P. F., McCann, F. E., Amjadi, P., Chang, C., McNamee, K., Tornehave, D., Haase, C., Agerso, H., Stennicke, V. W., Ahern, D., Ursø, B., Trowsdale, J., Feldmann, M., and Brennan, F. M. (2011) Blockade of NKG2D ameliorates disease in mice with collagen-induced arthritis: a potential pathogenic role in chronic inflammatory arthritis. *Arthritis Rheum.* **63,** 2617–2629 CrossRef Medline
38. Huang, W. C., Easom, N. J., Tang, X. Z., Gill, U. S., Singh, H., Robertson, F., Chang, C., Trowsdale, J., Davidson, B. R., Rosenberg, W. M., Fusai, G., Toubert, A., Kennedy, P. T., Peppa, D., and Maini, M. K. (2017) T cells infiltrating diseased liver express ligands for the NKG2D stress surveillance system. *J. Immunol.* **198,** 1172–1182 CrossRef Medline
39. Song, H., Kim, J., Cosman, D., and Choi, I. (2006) Soluble ULBP suppresses natural killer cell activity via down-regulating NKG2D expression. *Cell. Immunol.* **239,** 22–30 CrossRef Medline
40. Kloss, M., Decker, P., Baltz, K. M., Baessler, T., Jung, G., Rammensee, H. G., Steinle, A., Krusch, M., and Salih, H. R. (2008) Interaction of monocytes with NK cells upon Toll-like receptor–induced expression of the NKG2D ligand MICA. *J. Immunol.* **181,** 6711–6719 CrossRef Medline
41. Uhlenbrock, F., Hagemann-Jensen, M., Kehlet, S., Andresen, L., Pastorekova, S., and Skov, S. (2014) The NKG2D ligand ULBP2 is specifically regulated through an invariant chain-dependent endosomal pathway. *J. Immunol.* **193,** 1654–1665 CrossRef Medline
42. Gaidt, M. M., and Hornung, V. (2017) Alternative inflammasome activation enables IL-1β release from living cells. *Curr. Opin. Immunol.* **44,** 7–13 CrossRef Medline
43. Shimada, T., Park, B. G., Wolf, A. J., Brikos, C., Goodridge, H. S., Becker, C. A., Reyes, C. N., Miao, E. A., Aderem, A., Götz, F., Liu, G. Y., and Underhill, D. M. (2010) *Staphylococcus aureus* evades lysozyme-based peptidoglycan digestion that links phagocytosis, inflammasome activation, and IL-1β secretion. *Cell Host Microbe* **7,** 38–49 CrossRef Medline
44. Wolf, A. J., Reyes, C. N., Liang, W., Becker, C., Shimada, K., Wheeler, M. L., Cho, H. C., Popescu, N. I., Coggeshall, K. M., Arditi, M., and Underhill, D. M. (2016) Hexokinase is an innate immune receptor for the detection of bacterial peptidoglycan. *Cell* **166,** 624–636 CrossRef Medline
45. Bera, A., Biswas, R., Herbert, S., Kulauzovic, E., Weidenmaier, C., Peschel, A., and Götz, F. (2007) Influence of wall teichoic acid on lysozyme resistance in *Staphylococcus aureus*. *J. Bacteriol.* **189,** 280–283 CrossRef Medline
46. Bera, A., Herbert, S., Jakob, A., Vollmer, W., and Götz, F. (2005) Why are pathogenic staphylococci so lysozyme resistant?: The peptidoglycan *O*-acetyltransferase OatA is the major determinant for lysozyme resistance of *Staphylococcus aureus*. *Mol. Microbiol.* **55,** 778–787 CrossRef Medline
47. Wolf, A. J., Arruda, A., Reyes, C. N., Kaplan, A. T., Shimada, T., Shimada, K., Arditi, M., Liu, G., and Underhill, D. M. (2011) Phagosomal degradation increases TLR access to bacterial ligands and enhances macrophage sensitivity to bacteria. *J. Immunol.* **187,** 6002–6010 CrossRef Medline
48. Herskovits, A. A., Auerbuch, V., and Portnoy, D. A. (2007) Bacterial ligands generated in a phagosome are targets of the cytosolic innate immune system. *PLoS Pathog.* **3,** e51 CrossRef Medline
49. Lehrer, S. S., and Fasman, G. D. (1967) Fluorescence of lysozyme and lysozyme substrate complexes. Separation of tryptophan contributions by fluorescence difference methods. *J. Biol. Chem.* **242,** 4644–4651 Medline
50. Dahlquist, F. W., Jao, L., and Raftery, M. (1966) On the binding of chitin oligosaccharides to lysozyme. *Proc. Natl. Acad. Sci. U.S.A.* **56,** 26–30 CrossRef Medline
51. Müller, S., Wolf, A. J., Iliev, I. D., Berg, B. L., Underhill, D. M., and Liu, G. Y. (2015) Poorly cross-linked peptidoglycan in MRSA due to mecA induction activates the inflammasome and exacerbates immunopathology. *Cell Host Microbe* **18,** 604–612 CrossRef Medline
52. Battin, C., Hennig, A., Mayrhofer, P., Kunert, R., Zlabinger, G. J., Steinberger, P., and Paster, W. (2017) A human monocytic NF-κB fluorescent reporter cell line for detection of microbial contaminants in biological samples. *PLoS One* **12,** e0178220 CrossRef Medline
53. Xing, Y., Cao, R., and Hu, H. M. (2016) TLR and NLRP3 inflammasome-dependent innate immune responses to tumor-derived autophagosomes (DRibbles). *Cell Death Dis.* **7,** e2322 CrossRef Medline
54. O'Neill, L. A. (2011) A critical role for citrate metabolism in LPS signalling. *Biochem. J.* **438,** e5–e6 CrossRef Medline
55. Iacobazzi, V., and Infantino, V. (2014) Citrate: new functions for an old metabolite. *Biol. Chem.* **395,** 387–399 CrossRef Medline
56. Jha, A. K., Huang, S. C., Sergushichev, A., Lampropoulou, V., Ivanova, Y., Loginicheva, E., Chmielewski, K., Stewart, K. M., Ashall, J., Everts, B., Pearce, E. J., Driggers, E. M., and Artyomov, M. N. (2015) Network integration of parallel metabolic and transcriptional data reveals metabolic modules that regulate macrophage polarization. *Immunity* **42,** 419–430 CrossRef Medline
57. Infantino, V., Convertini, P., Cucci, L., Panaro, M. A., Di Noia, M. A., Calvello, R., Palmieri, F., and Iacobazzi, V. (2011) The mitochondrial citrate carrier: a new player in inflammation. *Biochem. J.* **438,** 433–436 CrossRef Medline
58. Infantino, V., Iacobazzi, V., Menga, A., Avantaggiati, M. L., and Palmieri, F. (2014) A key role of the mitochondrial citrate carrier (SLC25A1) in TNFα- and IFNγ-triggered inflammation. *Biochim. Biophys. Acta* **1839,** 1217–1225 CrossRef Medline
59. Infantino, V., Iacobazzi, V., Palmieri, F., and Menga, A. (2013) ATP-citrate lyase is essential for macrophage inflammatory response. *Biochem. Biophys. Res. Commun.* **440,** 105–111 CrossRef Medline
60. Palmieri, E. M., Spera, I., Menga, A., Infantino, V., Porcelli, V., Iacobazzi, V., Pierri, C. L., Hooper, D. C., Palmieri, F., and Castegna, A. (2015) Acetylation of human mitochondrial citrate carrier modulates mitochondrial citrate/malate exchange activity to sustain NADPH production during macrophage activation. *Biochim. Biophys. Acta* **1847,** 729–738 CrossRef Medline

61. Michelucci, A., Cordes, T., Ghelfi, J., Pailot, A., Reiling, N., Goldmann, O., Binz, T., Wegner, A., Tallam, A., Rausell, A., Buttini, M., Linster, C. L., Medina, E., Balling, R., and Hiller, K. (2013) Immune-responsive gene 1 protein links metabolism to immunity by catalyzing itaconic acid production. *Proc. Natl. Acad. Sci. U.S.A.* **110,** 7820–7825 CrossRef Medline
62. O'Neill, L. A., and Pearce, E. J. (2016) Immunometabolism governs dendritic cell and macrophage function. *J. Exp. Med.* **213,** 15–23 CrossRef Medline
63. Wellen, K. E., Hatzivassiliou, G., Sachdeva, U. M., Bui, T. V., Cross, J. R., and Thompson, C. B. (2009) ATP-citrate lyase links cellular metabolism to histone acetylation. *Science* **324,** 1076–1080 CrossRef Medline
64. Hatzivassiliou, G., Zhao, F., Bauer, D. E., Andreadis, C., Shaw, A. N., Dhanak, D., Hingorani, S. R., Tuveson, D. A., and Thompson, C. B. (2005) ATP citrate lyase inhibition can suppress tumor cell growth. *Cancer Cell* **8,** 311–321 CrossRef Medline
65. Berg, J. M., Tymoczko, J. L., and Stryer, L. (2002) *Biochemistry*, 5th Ed., W. H. Freeman, New York
66. Kurtoglu, M., Maher, J. C., and Lampidis, T. J. (2007) Differential toxic mechanisms of 2-deoxy-D-glucose versus 2-fluorodeoxy-D-glucose in hypoxic and normoxic tumor cells. *Antioxidants Redox Signal.* **9,** 1383–1390 CrossRef Medline
67. Lachmandas, E., Boutens, L., Ratter, J. M., Hijmans, A., Hooiveld, G. J., Joosten, L. A., Rodenburg, R. J., Fransen, J. A., Houtkooper, R. H., van Crevel, R., Netea, M. G., and Stienstra, R. (2016) Microbial stimulation of different Toll-like receptor signalling pathways induces diverse metabolic programmes in human monocytes. *Nat. Microbiol.* **2,** 16246 CrossRef Medline
68. Cohen, T. S., Boland, M. L., Boland, B. B., Takahashi, V., Tovchigrechko, A., Lee, Y., Wilde, A. D., Mazaitis, M. J., Jones-Nelson, O., Tkaczyk, C., Raja, R., Stover, C. K., and Sellman, B. R. (2018) *S. aureus* evades macrophage killing through NLRP3-dependent effects on mitochondrial trafficking. *Cell Rep.* **22,** 2431–2441 CrossRef Medline
69. Pearce, E. L., and Pearce, E. J. (2013) Metabolic pathways in immune cell activation and quiescence. *Immunity* **38,** 633–643 CrossRef Medline
70. Raud, B., Roy, D. G., Divakaruni, A. S., Tarasenko, T. N., Franke, R., Ma, E. H., Samborska, B., Hsieh, W. Y., Wong, A. H., Stüve, P., Arnold-Schrauf, C., Guderian, M., Lochner, M., Rampertaap, S., Romito, K., *et al.* (2018) Etomoxir actions on regulatory and memory T cells are independent of Cpt1a-mediated fatty acid oxidation. *Cell Metab.* **28,** 504–515.e7 CrossRef Medline
71. Gasser, S., Orsulic, S., Brown, E. J., and Raulet, D. H. (2005) The DNA damage pathway regulates innate immune system ligands of the NKG2D receptor. *Nature* **436,** 1186–1190 CrossRef Medline
72. Eissmann, P., Evans, J. H., Mehrabi, M., Rose, E. L., Nedvetzki, S., and Davis, D. M. (2010) Multiple mechanisms downstream of TLR-4 stimulation allow expression of NKG2D ligands to facilitate macrophage/NK cell crosstalk. *J. Immunol.* **184,** 6901–6909 CrossRef Medline
73. Hamerman, J. A., Ogasawara, K., and Lanier, L. L. (2004) Cutting edge: Toll-like receptor signaling in macrophages induces ligands for the NKG2D receptor. *J. Immunol.* **172,** 2001–2005 CrossRef Medline
74. Bertsche, U., Weidenmaier, C., Kuehner, D., Yang, S. J., Baur, S., Wanner, S., Francois, P., Schrenzel, J., Yeaman, M. R., and Bayer, A. S. (2011) Correlation of daptomycin resistance in a clinical *Staphylococcus aureus* strain with increased cell wall teichoic acid production and D-alanylation. *Antimicrob. Agents Chemother.* **55,** 3922–3928 CrossRef Medline
75. Bertsche, U., Yang, S. J., Kuehner, D., Wanner, S., Mishra, N. N., Roth, T., Nega, M., Schneider, A., Mayer, C., Grau, T., Bayer, A. S., and Weidenmaier, C. (2013) Increased cell wall teichoic acid production and D-alanylation are common phenotypes among daptomycin-resistant methicillin-resistant *Staphylococcus aureus* (MRSA) clinical isolates. *PLoS One* **8,** e67398 CrossRef Medline
76. Veiga, P., Bulbarela-Sampieri, C., Furlan, S., Maisons, A., Chapot-Chartier, M. P., Erkelenz, M., Mervelet, P., Noirot, P., Frees, D., Kuipers, O. P., Kok, J., Gruss, A., Buist, G., and Kulakauskas, S. (2007) SpxB regulates *O*-acetylation–dependent resistance of *Lactococcus lactis* peptidoglycan to hydrolysis. *J. Biol. Chem.* **282,** 19342–19354 CrossRef Medline
77. Kono, M., and Quastel, J. H. (1962) Effects of D-glucosamine and glucose analogues on glycogen biosynthesis *in vitro*. *Biochem. J.* **85,** 24–32 CrossRef Medline
78. Gao, W., Cameron, D. R., Davies, J. K., Kostoulias, X., Stepnell, J., Tuck, K. L., Yeaman, M. R., Peleg, A. Y., Stinear, T. P., and Howden, B. P. (2013) The RpoB H_{481} rifampicin resistance mutation and an active stringent response reduce virulence and increase resistance to innate immune responses in *Staphylococcus aureus*. *J. Infect. Dis.* **207,** 929–939 CrossRef Medline
79. He, Y., Hara, H., and Núñez, G. (2016) Mechanism and regulation of NLRP3 inflammasome activation. *Trends Biochem. Sci.* **41,** 1012–1021 CrossRef Medline
80. Andresen, L., Jensen, H., Pedersen, M. T., Hansen, K. A., and Skov, S. (2007) Molecular regulation of MHC class I chain-related protein A expression after HDAC-inhibitor treatment of Jurkat T cells. *J. Immunol.* **179,** 8235–8242 CrossRef Medline
81. Souvorov, A., Agarwala, R., and Lipman, D. J. (2018) SKESA: strategic k-mer extension for scrupulous assemblies. *Genome Biol.* **19,** 153 CrossRef Medline
82. Li, H., and Durbin, R. (2009) Fast and accurate short read alignment with Burrows–Wheeler transform. *Bioinformatics* **25,** 1754–1760 CrossRef Medline
83. Carver, T., Harris, S. R., Berriman, M., Parkhill, J., and McQuillan, J. A. (2012) Artemis: an integrated platform for visualization and analysis of high-throughput sequence-based experimental data. *Bioinformatics* **28,** 464–469 CrossRef Medline
84. Monk, I. R., Tree, J. J., Howden, B. P., Stinear, T. P., and Foster, T. J. (2015) Complete bypass of restriction systems for major *Staphylococcus aureus* lineages. *mBio* **6,** e00308-15 CrossRef Medline
85. Guérillot, R., Li, L., Baines, S., Howden, B., Schultz, M. B., Seemann, T., Monk, I., Pidot, S. J., Gao, W., Giulieri, S., Gonçalves da Silva, A., D'Agata, A., Tomita, T., Peleg, A. Y., Stinear, T. P., *et al.* (2018) Comprehensive antibiotic-linked mutation assessment by resistance mutation sequencing (RM-seq). *Genome Med.* **10,** 63 CrossRef Medline
86. Zhang, Y., Werling, U., and Edelmann, W. (2012) SLiCE: a novel bacterial cell extract-based DNA cloning method. *Nucleic Acids Res.* **40,** e55–e55 CrossRef Medline
87. Aldana, B. I., Zhang, Y., Lihme, M. F., Bak, L. K., Nielsen, J. E., Holst, B., Hyttel, P., Freude, K. K., and Waagepetersen, H. S. (2017) Characterization of energy and neurotransmitter metabolism in cortical glutamatergic neurons derived from human induced pluripotent stem cells: a novel approach to study metabolism in human neurons. *Neurochem. Int.* **106,** 48–61 CrossRef Medline
88. Vohra, R., Aldana, B. I., Skytt, D. M., Freude, K., Waagepetersen, H., Bergersen, L. H., and Kolko, M. (2018) Essential roles of lactate in Müller cell survival and function. *Mol. Neurobiol.* **55,** 9108–9121 CrossRef Medline
89. Mawhinney, T. P., Robinett, R. S., Atalay, A., and Madson, M. A. (1986) Gas-liquid chromatography and mass spectral analysis of mono-, di- and tricarboxylates as their *tert*-butyldimethylsilyl derivatives. *J. Chromatogr.* **361,** 117–130 CrossRef Medline
90. Biemann, K. (1962) *Mass Spectrometry in Organic Chemistry Applications*, McGraw, New York
91. Sellick, C. A., Croxford, A. S., Maqsood, A. R., Stephens, G. M., Westerhoff, H. V., Goodacre, R., and Dickson, A. J. (2015) Metabolite profiling of CHO cells: molecular reflections of bioprocessing effectiveness. *Biotechnol. J.* **10,** 1434–1445 CrossRef Medline
92. Smart, K. F., Aggio, R. B., Van Houtte, J. R., and Villas-Bôas, S. G. (2010) Analytical platform for metabolome analysis of microbial cells using methyl chloroformate derivatization followed by gas chromatography-mass spectrometry. *Nat. Protoc.* **5,** 1709–1729 CrossRef Medline
93. Johnsen, L. G., Skou, P. B., Khakimov, B., and Bro, R. (2017) Gas chromatography–mass spectrometry data processing made easy. *J. Chromatogr. A* **1503,** 57–64 CrossRef Medline